Check for updates

²³⁸U/²³⁵U measurement in single-zircon crystals: implications for the Hadean environment, magmatic differentiation and geochronology†

François L. H. Tissot, [ID] *[ab] Mauricio Ibanez-Mejia, [ID] [c] Patrick Boehnke,[de] Nicolas Dauphas,[d] David McGee,[a] Timothy L. Grove[a] and T. Mark Harrison[f]

Owing to the challengingly small amounts of uranium (U) they contain, the isotopic composition (²³⁸U/²³⁵U) of single zircon grains has never been measured. Leveraging methods we designed for analysis of small sample amounts and modern MC-ICPMS instruments, we show that precise ($\pm$0.04 to $\pm$0.25‰) single-zircon ²³⁸U/²³⁵U measurements are now possible. We report data for 31 single grains from the Jack Hills conglomerate, and 3 reference zircon localities (FC-1, R33 and Temora). Consistent with the reducing conditions implied by the small Ce anomalies of many Hadean zircon, Jack Hills grains display only small δ^{238}U variations (from -0.60 to -0.12‰). The distribution is centered on the average chondritic and bulk continental crust value, arguing against the widespread existence of Oklo-type reactors in the early Earth. The subtle δ^{238}U variations in Jack Hills zircons are more plausibly explained by a small ($\sim$0.10%) mass-dependent equilibrium isotope fractionation between at least one U-bearing accessory mineral and silicate melts, during magmatic differentiation under reducing conditions. In contrast, the large δ^{238}U difference between pooled titanite and pooled zircon fractions from the Fish Canyon Tuff sample suggests larger isotope effects during igneous fractional crystallization under oxidizing conditions ($\sim$QFM+2), with preferential removal of ²³⁵U from the melt and into zircon, and/or other accessory phases. We estimate that $\sim$50% of zircon dated by the CA-ID-TIMS method would be amenable to single-grain U isotope measurements, making this method widely applicable to future studies. This would enable (i) improvements in precision and accuracy of U–Pb and Pb–Pb dates, (ii) accurate investigation of U-series disequilibrium contribution to U–Pb discordance, and (iii) accurate re-evaluation of U decay constants.

1. Introduction

Earth's known rock record only extends to ~4.05 Ga (ref. 1). As the only older lithic record, detrital zircons are thus key to understanding the development of crustal rocks and surface environments during the Hadean,[2,3] an eon which presumably saw the waning of the extraterrestrial bombardment,[4,5] the

[a]Department of the Earth, Atmospheric and Planetary Sciences, Massachusetts Institute of Technology, Cambridge, MA 02139, USA

[b]The Isotoparium, Division of Geological and Planetary Sciences, California Institute of Technology, Pasadena, CA 91125, USA. E-mail: tissot@caltech.edu

[c]Department of Earth and Environmental Sciences, University of Rochester, Rochester, NY 14608, USA

[d]Department of the Geophysical Sciences, The University of Chicago, Chicago, IL 60637, USA

[e]Chicago Center for Cosmochemistry, Chicago, IL, USA

[f]Department of Earth, Planetary, and Space Sciences, University of California, Los Angeles, CA 90095, USA

† Electronic supplementary information (ESI) available: Additional notes on Materials and methods, supplementary text, Fig. S1–S11, Tables S1–S5. See DOI: 10.1039/c9ja00205g

emergence of life,[6,7] and the establishment of continents.[2,8] Numerous chemical and isotopic proxies have therefore been investigated in Hadean zircons and their inclusions (review in ref. 3) but owing to the small size of typical zircon crystals (<10–50 μg), and the even smaller size of Hadean grains (~1 μg), geochemical studies are limited to the main constituents of, and minor/trace elements partitioning strongly into, zircons. While uranium (U) concentrations are routinely measured in zircons for U–Pb geochronology, the U isotopic composition of single-zircon grains has never been measured. Indeed, significant analytical challenges are associated with the analysis of the small amounts of U contained by individual crystals, which are invariably regarded as insufficient to allow for the precise determination of ²³⁸U/²³⁵U ratios.[9–12]

Building on and improving upon methodologies we developed to precisely and accurately determine the ²³⁸U/²³⁵U of small samples,[13] we show that modern Multi-Collector ICPMS instruments provide sufficient precision to resolve U isotopic differences between single zircon grains. We present a detailed description of these analytical methods, and report data for 31 single grains from the Jack Hills conglomerate (Western

This journal is © The Royal Society of Chemistry 2019

J. Anal. At. Spectrom., 2019, **34**, 2035–2052 | **2035**

Australia) and 3 reference zircon localities. Using data obtained on Jack Hills zircons we assess whether natural nuclear reactors were present in the Hadean, the possible causes of fractionation in magmatic settings, and the implications for high-precision U–Pb and Pb–Pb geochronology. Finally, we discuss the current limitations and future improvements that could help make single-zircon $^{238}U/^{235}U$ determinations more accurate, precise, and practical for a variety of applications in geochemistry and geochronology.

2. Motivations

There are several reasons why quantifying the $^{238}U/^{235}U$ of single zircons, and Hadean ones in particular, is important:

(1) Oklo-type natural nuclear reactors may have been more prevalent in the Hadean,[14] when ^{235}U abundance was above the ~3% threshold required for self-sustained neutron-induced fission (~17% at 4 Ga and ~25% at 4.5 Ga). So far, the Oklo U ore deposit (Gabon), which reached criticality ~1.78 Ga, is the only known natural reactor. In the reactor zones, neutron-induced ^{235}U fission led to $^{238}U/^{235}U$ increases that often reached +100 to +475‰ (ref. 15). These isotopic variations are 100× larger than those documented in other geological settings, which only range from −4.1 to +4.8‰ (ref. 16 and 17). It is thus conceivable that if Oklo-type reactors were common in the Hadean, even small amounts of highly anomalous U isotope composition could have contaminated sediments and igneous rocks and potentially be recorded in Hadean zircons.

(2) While stable isotopic variations were originally thought to be confined to low-T settings and light elements, many studies have now documented variations in high-T settings for heavy elements, reflecting both equilibrium and kinetic processes (review in ref. 18). For U, mass-dependent isotope fractionations ($\propto 1/T^2$) should be small at magmatic temperatures (~−0.07‰ at 850 °C), but nuclear volume effects[19] ($\propto 1/T$) could induce larger U isotopic fractionations (~+0.61‰ at 850 °C). At this writing, the U isotopic systematics of igneous rocks is still in its infancy (review in ref. 17), but the available data suggests the existence of mineral specific U isotope effects,[9,11,12] which can result in magmatic differentiation trends, as observed in angrite meteorites.[20] Based on studies of different isotopic systems, the potential drivers of U isotope fractionation in magmatic settings would be temperature, the nature of the minerals sequestering U, the redox state of the melt, and the extent of crystallization.

(3) Uranium isotopic variations can affect the accuracy and precision of U–Pb and Pb–Pb dates.[9,16,20,21] Establishing a timeline for the dramatic biological/environmental changes that punctuated Earth's history relative to their potential triggers (*e.g.*, asteroid impacts, large igneous province emplacements) requires, however, highly precise and accurate absolute ages.[22–26] These ages are typically obtained using U–Pb and/or Pb–Pb dates of zircons found within ash layers/lavas associated with the events of interest. Based on the limited U isotope variability (~0.7‰) observed in pooled zircons (*i.e.*, multi-grain dissolutions) of different ages and localities, a recommended $^{238}U/^{235}U$ was established for accessory-phase geochronology.[9,12] This approach assumes that the recommended value encompasses all $^{238}U/^{235}U$ variability in natural zircon, such that age accuracy after uncertainty propagation is not compromised. The central limit theorem, however, predicts that pooled zircons should display less scatter in their $^{238}U/^{235}U$ than single zircon grains (Fig. 1). Therefore, the only robust way to quantify $^{238}U/^{235}U$
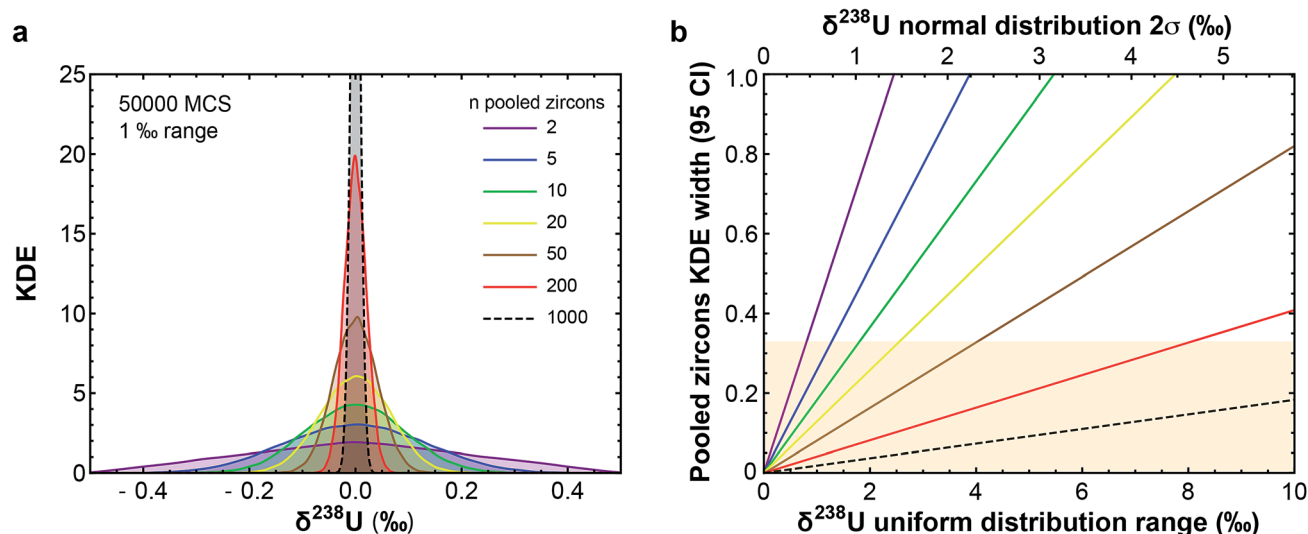

Fig. 1 (a) Kernel Density Estimator (KDE) of the U isotope composition of *n* pooled zircons randomly picked from a uniform distribution centered on $\delta^{238}U = 0$ and of total range, 1‰. KDEs are built using 50 000 randomly generated sets (Monte-Carlo Simulations, MCS) of *n* zircons, with *n* between 2 and 1000. (b) Width (95% confidence interval) of the KDE of *n* pooled zircons predicted by the central limit theorem as a function of the dispersion in the $\delta^{238}U$ distribution from which the grains are randomly picked (lower *x*-axis, range covered by a uniform distribution; upper *x*-axis, 2σ of a normal distribution). For *n* zircons picked within a distribution of variance σ^2, the variance of the mean $\delta^{238}U$ of the *n* zircons tends toward $\sigma_{mean}^2 = \sigma^2/n$. The uncertainty on the recommended $^{238}U/^{235}U$ for use in geochronology (yellow horizontal band) is based on the analysis of hundreds to thousands of pooled zircons[9,12] and could theoretically hide a true $\delta^{238}U$ variability of greater than 10‰ in individual zircons.

2036 | *J. Anal. At. Spectrom.*, 2019, **34**, 2035–2052

This journal is © The Royal Society of Chemistry 2019

variability in natural zircons is *via* single-grain U isotope analysis, without which sub-permil accuracy and precision in U–Pb and Pb–Pb geochronology is, *a priori*, not possible.

3. Samples

To explore $^{238}U/^{235}U$ variability between single zircon grains, we selected 3 reference zircon localities (FC-1, R33 and Temora; $^{206}Pb/^{238}U$ ages between 418 and 1095 Ma; ref. 27) and 31 Jack Hills zircon crystals with apparent $^{207}Pb/^{206}Pb$ dates between ~3.3 and 4.2 Ga (ref. 28). As all Jack Hills crystals formed before oxidative conditions could solubilize U in water as U^{VI} (ref. 29), their composition should be purely controlled by magmatic processes and/or U contributions from Oklo-type reactors. Resolvable U isotope variations in such samples would thus imply that systematic investigation of $^{238}U/^{235}U$ ratios could provide further insight into the magmatic history of individual detrital zircons, which otherwise lack geological context.

4. Methods

All Teflon labware (*i.e.*, PFA vials and beakers from Savillex) was pre-cleaned 3× with boiling aqua regia (3 : 1 mixture of HCl : HNO_3), followed by boiling Milli-Q water. Glass vials were cleaned with acetone and MQ water. Centrifuge tubes were leached with 50% (vol) HCl overnight and/or rinsed 3× with MQ water.

4.1. Direct zircon dissolution

Zircon dissolution followed a protocol adapted from those used in geochronology studies.[30,31] Single zircon crystals were pipetted into clean Teflon beakers and cleaned by successive leaching in HCl (16 drops of 6.2 M) and HNO_3 (16 drops of 5 M) on a hotplate at ~90–100 °C for 30–60 min. These steps aimed at removing any iron oxide coatings, secondary alteration products and/or adsorbed U present at the surface of the grains or in small factures within them. After each leaching step, the grains were sonicated in a hot water bath for 10 min, and the acid solution was transferred to a 2 mL plastic vial. The solution recovered was used to check the amount of U released in each step (Table S1†). Each grain was further rinsed with 10 drops of MQ, which were also collected and added to the leachate solution, before complete dry-down of the grains at 130 °C on hotplate. After cleaning, the grains were transferred to Teflon micro-capsules and immersed in 3 drops (~75 μL) of 28 M HF. The micro-capsules were then placed on a Teflon holder accommodating up to 18 capsules, itself placed inside a high-volume Parr® acid digestion vessel and into an oven at 210 °C for 48 h. After the HF dissolution step, the samples were dried and converted to HCl by addition of 3 drops of 6.2 M HCl and placed back in the Parr vessel and in the oven at 180 °C for 24 h.

4.2. Zircon chemical abrasion followed by dissolution

To assess the effects of thermal annealing and chemical abrasion on $^{238}U/^{235}U$ ratios, six of the Jack Hills samples were treated with the chemical abrasion method,[30] which selectively dissolves radiation damaged subdomains that have may have

not remained closed systems for U and Pb isotopes (as leach-ates), and leaves behind crystalline domains more likely to have remained in closed-systems (as residues). After the HCl and HNO_3 cleaning steps, zircons were annealed in quartz vials at 900 °C for 62 h using a Thermolyne benchtop muffle furnace, transferred to Teflon micro-capsules, and chemically abraded with 28 M HF at 210 °C for 7 h 45 min (in a Parr vessel). The abrasion solutions were collected in clean 7 mL Teflon beakers and the grains were rinsed twice with 8 drops of MQ, which was also collected and added to the leachate solution. The undigested part of the zircons (*i.e.*, residues) were again covered with 3 drops (~75 μL) of concentrated HF and placed back in the Parr vessel and in the oven at 210 °C for 48 h to achieve complete digestion of the residues. After the HF dissolution step, conversion to a chloride matrix was done by adding 3 drops of 6.2 M HCl and placing the Parr vessel at 180 °C for 24 h. The solutions containing the fully digested residue thus obtained were finally transferred to clean 7 mL Teflon beakers.

4.3. Uranium concentration measurements and spiking

After digestion, all sample solutions (from cleaning, direct dissolution, chemical abrasion and residue digestion) were dried down completely and re-dissolved in 3 mL of 3 M HNO_3. A 2% aliquot (60 μL) was spiked with ~0.65 ng of IRMM-3636 double-spike (50.46% of ^{233}U and 49.51% of ^{236}U; ref. 32), diluted with 0.3 M HNO_3 to a total volume of 750 μL, and measured using a Nu-Plasma II MC-ICPMS (McGee lab) to determine the amount of U in each sample (Table S1†). Enough IRMM-3636 was then added to each sample to obtain a U_{spike}/U_{sample} ratio of ~3–4%: a value recommended by Weyer *et al.*[33] to minimize spike consumption, abundance sensitivity effect of ^{238}U onto ^{236}U, as well as contribution from amplifier noise and counting statistic on ^{233}U and ^{236}U to the measurement uncertainty. To ensure full homogenization of the sample-spike mixture, all samples were completely dried down on hot plate at 150 °C, taken back in 1 mL of concentrated HNO_3, evaporated to near dryness and taken back into 2.5 mL of 3 M HNO_3 + 0.02 M oxalic acid. The dilute oxalic acid was used to solubilize Zr[34] and prevent retention of Zr (which makes up ~50 wt% of the matrix of zircons) during column chemistry.

4.4. Uranium purification for Zr rich samples

Uranium purification was done on U/Teva resin, following a procedure modified from Tissot and Dauphas[16] (Table 1). Given the small mass of U (~1–50 ng) and the large Zr/U atomic ratio of the samples (~481 for a zircon assuming typical Zr and U concentrations of, respectively, 48 wt% and 2600 ppm, ref. 35), two main modifications were brought to the procedure: (i) a more extensive column cleaning was done to minimize blank contribution from the column, and (ii) sample loading and matrix rinsing used 3 M HNO_3 + 0.02 M oxalic acid, as oxalic acid solubilizes Zr.[34] The procedure was repeated twice to ensure complete matrix removal. The purified U cuts were then evaporated completely at 175 °C, covered with 0.5–1 mL of HNO_3/H_2O_2 (1 : 1) and dried completely to remove residual

This journal is © The Royal Society of Chemistry 2019

J. Anal. At. Spectrom., 2019, **34**, 2035–2052 | **2037**

Table 1 Chromatographic extraction protocol of U in zircons on U/Teva resin. Column volume (cv) = 2 mL

Column #1				Column #2		
Step	Acid type	Volume	Comment	Acid type	Volume	Comment
Cleaning	0.05 M HCl	40 mL		0.05 M HCl	40 mL	
Conditioning	3 M HNO$_3$ + 0.02 M oxalic acid	10 mL		3 M HNO$_3$ + 0.02 M oxalic acid	10 mL	
Sample loading	3 M HNO$_3$ + 0.02 M oxalic acid	2.5 mL		3 M HNO$_3$ + 0.02 M oxalic acid	2.5 mL	
Matrix rinse	3 M HNO$_3$ + 0.02 M oxalic acid	12 mL	Elution of matrix except U, Th, Np	3 M HNO$_3$ + 0.02 M oxalic acid	6 mL	Elution of remaining Zr
				3 M HNO$_3$	6 mL	Oxalic rinse
Conversion to HCl	10 M HCl	5 mL		10 M HCl	5 mL	
Th rinse	5 M HCl	8 mL	Elution of Th	5 M HCl	8 mL	Elution of remaining Th
Elution	0.05 M HCl	15 mL	U is recovered	0.05 M HCl	15 mL	U is recovered

organics, before being taken back in 2 mL of concentrated HNO$_3$ and left on the hotplate overnight at 140 °C to ensure full re-dissolution of the sample.

4.5. Yield, blanks and purity checks

For each sample, a 1.5% solution aliquot (30 μL) was taken post-column chemistry, diluted with 380 μL of 0.3 M HNO$_3$, and measured by MC-ICPMS to determine U recovery and Zr/U ratio in the purified solution. Yields, calculated as the ratio of U in the sample solution before and after column chemistry, were between 80 and 98%. The Zr/U atomic ratios varied mostly between 0.1 and 1.2, with four samples showing Zr/U between 1.4 and 6.4 (Table S2†). Given the typical zircon Zr/U atomic ratio of ~481, these values indicate that ~99–100% of the Zr was removed during sample purification. The procedural blank was 0.005–0.017 ng U (~0.002 to 0.7% of sample uranium) and is therefore negligible.

4.6. Mass spectrometry

Uranium isotope analyses were performed on two MC-ICPMS instruments: a Nu-Plasma II-ES in the McGee lab (MIT) and a Thermo Finnigan Neptune upgraded to Neptune Plus specifications at the Origins Lab (University of Chicago). The Nu-II was equipped with high-sensitivity dry plasma cones (Ni sampler cones 319–646, Ni skimmer cones 325–294) and sample introduction was done using an Aridus II desolvating nebulizer, yielding a sensitivity of ~0.75–1.0 V ppb^{-1} on ^{238}U for a sample flow rate of 100 μL min^{-1}. The Neptune was equipped with a set of Jet sample cones and X-skimmer cones and the sample introduction was also done using an Aridus II, yielding a sensitivity of ~1.5–1.7 V ppb^{-1} on ^{238}U for a sample flow rate of 100 μL min^{-1}. The measurements were done in low-resolution mode using static cup configurations (Table 2), and typically comprised 50 or 60 cycles of 4.194 s integration time each. Take up time was set to 60 seconds and rinse time between 450 and 550 seconds were used.

Due to the large dynamic range of the U system (^{238}U/^{235}U ~137.8), measurements at low concentration are counting

Table 2 Cup configurations for U isotopic measurements by MC-ICPMS in low resolution mode

Isotope	^{232}Th	^{233}U	^{234}U	^{235}U	^{236}U	^{238}U
Neptune Plus (U. of Chicago)						
Cup	L2	L1	Axial	H1	H2	H3
Resistor (Ω)	10^{11}	10^{11}	SEM	10^{11}	10^{11}	10^{11}
Nu-Plasma II-ES (MIT)						
Cup	L4	L3	L2	L1	Axial	H2
Resistor (Ω)	10^{11}	10^{11}	10^{11}	10^{11}	10^{11}	10^{11}

statistics limited. To achieve high-precision on small samples loads, the volume of solution was adjusted to obtain a signal of at least 10 V on ^{238}U (and ~77 mV on ^{235}U). Following this protocol, measurements were done at U concentrations between 6.5 and 12 ppb, sometimes in as little as 0.25 mL of solution. Signal intensities were thus between 10 and 20 V for ^{238}U, 165 and 275 mV for ^{236}U and ^{233}U, 77 and 145 mV for ^{235}U, 0.6 to 1.2 mV for ^{234}U (when measured on the Nu-II) and ~31 000 and 60 000 cps for ^{234}U (when measured on the axial secondary electron multiplier (SEM) on the Neptune). Estimation of the Neptune "cps-to-volt" conversion factor was done once a week by measuring the ^{236}U/^{238}U in a CRM-112a solution spiked with the IRMM-3636 U double-spike using two different cup configurations: first with both ^{236}U and ^{238}U on Faraday cups, then with ^{236}U on the axial SEM and ^{238}U on a Faraday cup (for more details, see Table S4 in ref. 16). Thorium-232 was monitored during each analysis and the signal was found to be always below 10 mV. Given the extremely low rate of hydride formation relevant to the measurements (~7 × 10^{-7}; ref. 16), the residual amount of Th in the sample has virtually no effect on the U isotope analysis. This is clearly demonstrated by replicate analyses of the BCR-2 standard (Fig. 2a and Table S3†), where ^{232}Th signals varied between 0.04 and 2.9 mV, with no impact on either the accuracy or the precision of the U isotope data obtained. Baseline measurements and amplifier gain calibrations were done at least daily.
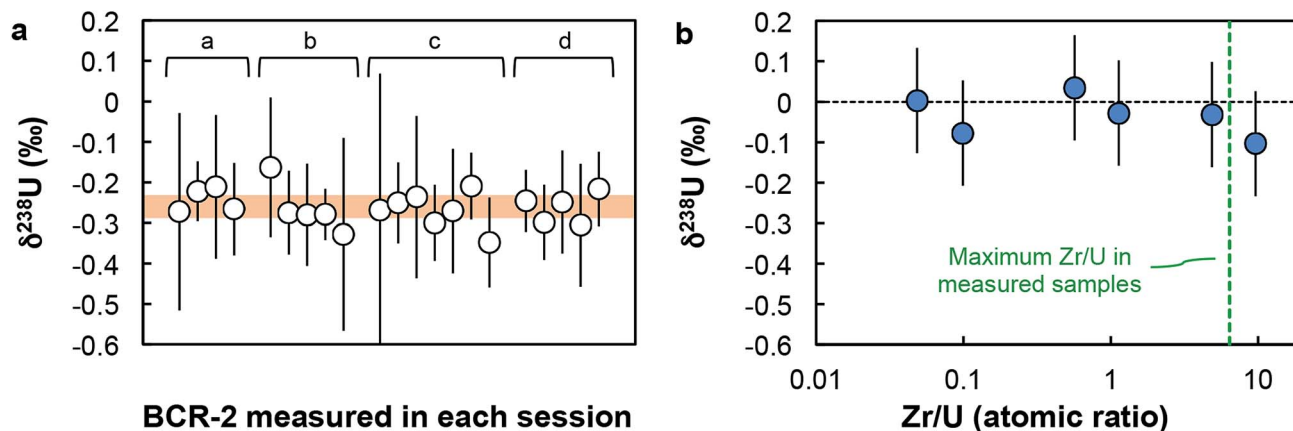
2038 | *J. Anal. At. Spectrom.*, 2019, **34**, 2035–2052

This journal is © The Royal Society of Chemistry 2019

Fig. 2 Accuracy tests. (a) $\delta^{238}U$ values for geostandard BCR-2 measured during each analytical session (letters a to d refer to sample replicates, see Table S3†). Each data point was acquired using a similar number of solution analyses as the one used for zircons (n between 1 and 8). Every measurement is within error of the recommended average value (orange band) of $-0.27 \pm 0.05\permil$ (95% CI). (b) $\delta^{238}U$ values measured on Zr-doped CRM-112a solutions vs. Zr/U (atomic) ratios of the doped solutions. All solutions give $\delta^{238}U$ values within uncertainty of $0\permil$, indicating the absence of resolvable matrix effect.

4.7.   Instrumental mass bias correction and data reduction

Isotope mass fractionation introduced during chemical separation and mass spectrometry was corrected for using the ^{233}U–^{236}U IRMM-3636 double-spike and the data reduction methodology described in details in Tissot and Dauphas.[16] In brief, the raw signals are corrected for: (i) on peak zero, (ii) ^{238}U tail contribution onto ^{236}U, ^{235}U, and ^{234}U signals (respectively, 0.6×10^{-6}, 0.25×10^{-6}, and 0.1×10^{-6} of the ^{238}U signal intensity), (iii) hydride formation, and (iv) the decay of the spike isotopes (^{233}U and ^{236}U) between the time of spike calibration and sample analysis. The cup configuration and the set of cones used can result in systematic offsets of up to $0.20\permil$ in the final $^{238}U/^{235}U$ measured.[16] To account for this, every sample was bracketed by measurements of the CRM-112a standard spiked with IRMM-3636 at the same level as the samples. For sample limited analyses, only 18 to 42 cycles could be obtained and the bracketing standard measurements used to calculate the uncertainty were truncated to match the number of cycles measured on the sample.

5.   Results

5.1   Notations

U isotope compositions are reported as $\delta^{238}U$ values relative to the U standard CRM-112a (also named SRM960 or NBL112-a; CRM-145 for the solution form):

$$\delta^{238}U = [(^{238}U/^{235}U)_{sample}/(^{238}U/^{235}U)_{CRM\text{-}112a} - 1] \times 10^3. \quad (1)$$

All absolute ratios, including literature data, are calculated assuming $^{238}U/^{235}U = 137.837 \pm 0.015$ for CRM-112a (ref. 36). This value results from an inter-laboratory calibration effort in which different instruments (i.e., MC-ICPMS and TIMS), reference materials (i.e., IRMM-3636, IRMM-072/15, in-house spikes calibrated against IRMM-074/10 or IRMM-184) and instrumental fractionation correction methods were used. This value is

therefore preferred over the often used value of 137.829 ± 0.022 from ref. 9, which was obtained using a single instrument and spike. Uncertainties are reported as "2SE external reproducibility" and calculated as $2 \times \sigma_{standard}/\sqrt{n}$, where $2 \times \sigma_{standard}$ is the 2 S.D. daily external reproducibility of repeat measurements of CRM-112a bracketed by itself (measured at the same concentration as the sample), and n is the number of repeat analyses of the same sample solution (typically $n = 2$–4).

5.2   Data accuracy and precision

Given the analytical challenges posed by the analysis of the low U loads of single zircons (1–50 ng of U), a comprehensive series of precision and accuracy tests were performed (additional details in ESI†).

(i) Accuracy test. Four replicates of the Columbia River basalt (BCR-2) were processed and measured with the zircon samples. For each replicate, the average $\delta^{238}U$ obtained are both reproducible ($-0.23 \pm 0.06\permil$, $-0.27 \pm 0.05\permil$, $-0.27 \pm 0.04\permil$ and $-0.26 \pm 0.04\permil$) and indistinguishable from the average value of $-0.27 \pm 0.05\permil$ (95% CI), based on data from 11 studies (see ESI† in ref. 16). Furthermore, the $\delta^{238}U$ values measured during each daily session, with a similar number of solution analyses as the one used for zircons (n between 1 and 8), are all within uncertainty of the average value (Fig. 2a).

(ii) Zr doping test. To test whether the residual Zr present in the purified U fractions could result in systematic bias of the $^{238}U/^{235}U$ analyses, spiked aliquots of CRM-112a were doped with Zr and measured as "unknown" samples. The $\delta^{238}U$ obtained on Zr-doped CRM-112a solutions are indistinguishable from $0\permil$ (Fig. 2b), indicating that the presence of Zr at the levels tested does not affect the U isotope measurements.

(iii) Matrix effects. As the IRMM-3636 double-spike consists almost entirely of ^{233}U and ^{236}U, the presence of matrix effects can be investigated by checking the agreement between the $\delta^{238}U_{DS+SSB}$ values, obtained from the double-spike data reduction, and the $\delta^{238}U_{SSB}$ values, obtained from the raw
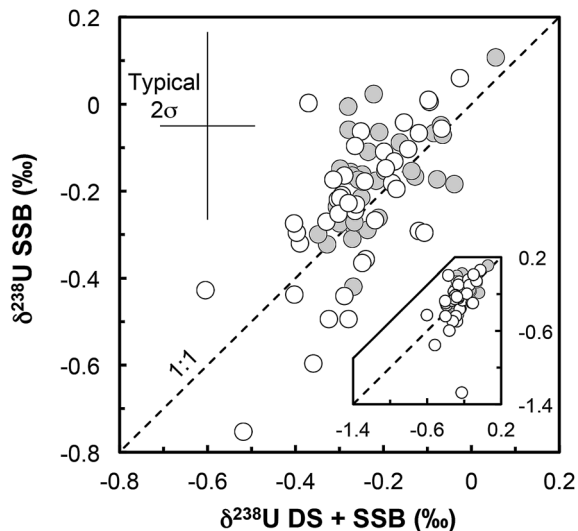
Fig. 3 $\delta^{238}U$ values obtained with the double-spike data reduction method (DS + SSB, *x*-axis) plotted against the raw values measured, striped of the minor ^{235}U and ^{238}U spike contribution (SSB, *y*-axis). All values are standard bracketed (SSB). The agreement of the two sets of values indicates that no resolvable matrix effects affected the measurements (for more details see ref. 16). Grey circles: geo-standards; white circles: zircons.

$^{238}U/^{235}U$ (striped of the spike ^{235}U and ^{238}U contribution and corrected only for on peak zero, hydride formation and tailing of ^{238}U onto lighter isotopes) bracketed by standard measurements (SSB).[16,37] For all but one sample (Fig. 3) there is a very good agreement between these values ($\delta^{238}U_{DS} - \delta^{238}U_{SSB}$ is $-0.04‰$ on average), indicating that matrix effect did not affect the measurements (except possibly RSES72-18.10 residue).

(iv) *Reference zircons.* Perhaps the most telling evidence of the reliability of our dataset is the excellent agreement of our reference zircon data with that of Hiess *et al.*[9] and Livermore

et al.[12] Samples FC-1, R33 and Temora were measured both here and in at least one of these previous studies, and yield identical $\delta^{238}U$ values (Fig. 4a). In the present work, analyses were performed with only 7–17 ng of U, while the data from Livermore *et al.*[12] and Hiess *et al.*[9] used 400–801 and 6000–23 000 ng of U from pooled zircons, respectively (Fig. 4b).

(v) *Achievable precision.* The precision of our measurements is in excellent agreement with the lower limit theoretically achievable by MC-ICPMS (grey curves, Fig. 4b). The theoretical curves correspond to the quadratic sum of the counting statistics and Johnson noise uncertainties for $^{238}U/^{235}U$ measured with a $^{233}U–^{236}U$ double spike on Neptune MC-ICPMS, calculated as (see derivation in the ESI†):

$$\sigma_{\delta238/235'*}^2 \simeq 10^6 \left\{ \frac{1}{n_8} \left[1 + R_U + \frac{2}{p} \left(\frac{\mu_{8/5}}{\mu_{6/3}} \right)^2 \right] + \frac{1}{n_8^2} \right.$$

$$\left. \left[\sigma_{J8}^2 + \sigma_{J5}^2 R_U^2 + 2 \frac{\sigma_{J6}^2}{p^2} \left(\frac{\mu_{8/5}}{\mu_{6/3}} \right)^2 \right] \right\} \times \sqrt{2}, \quad (2)$$

where n_8 is the total number of ^{238}U atoms reaching the detector, R_U is the $^{238}U/^{235}U$ of the sample (which can be taken as the average crustal ratio of 137.797, ref. 16), p is the is $^{236}U/^{238}U$ in the measured solution (sample + spike), $\mu_{j/i}$ is equal to $\ln(m_j/m_i)$, with m_i the mass of isotope i, and σ_{Ji}^2 is the Johnson noise uncertainty associated with measurement of the isotope i beam.

5.3 Variable $^{238}U/^{235}U$ between single zircon grains

Our dataset shows that single-zircon $^{238}U/^{235}U$ variations exist and can be resolved by high-precision MC-ICPMS measurements (Fig. 5). Individual zircons have $\delta^{238}U$ values between $-0.52 \pm 0.17‰$ (RSES72-2.2) and $-0.12 \pm 0.06‰$ (RSES72-6.1) and chemically abraded samples show similar variations, with

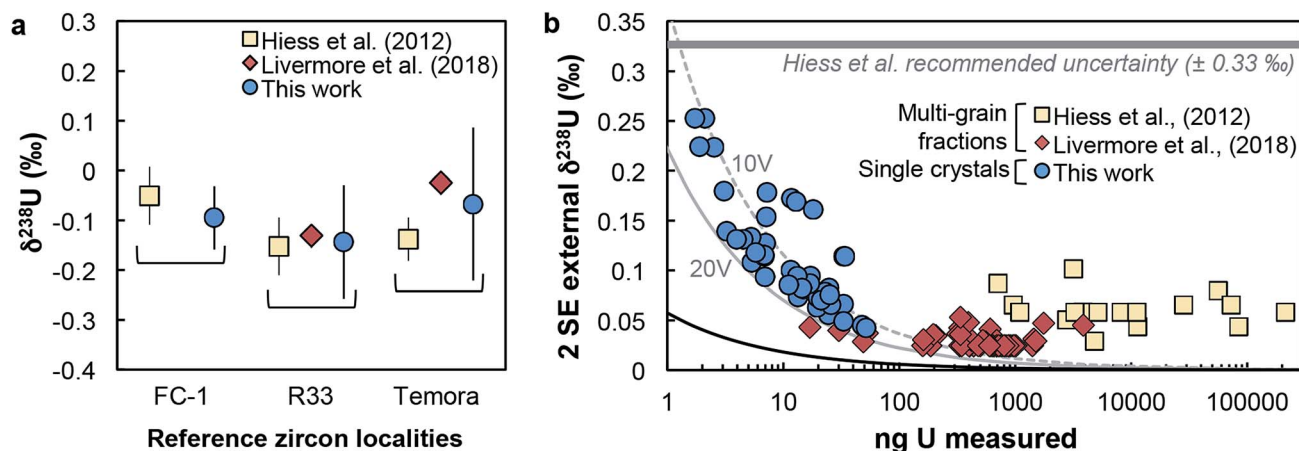**Fig. 4** (a) Comparison of $\delta^{238}U$ values obtained on single-zircon grains (circles, this work) and pooled zircons (squares: ref. 9; diamonds: ref. 12) for 3 reference zircon localities. (b) Uncertainty on $\delta^{238}U$ values *vs.* amount of U measured (in ng). Uncertainties are 2 SE external reproducibility (see Section 5.1). Grey curves show the theoretical lower limit achievable, calculated with eqn (2), assuming measurements on a Neptune MC-ICPMS with 2.5% ion transmission and ^{238}U measured at 10 V (dashed grey curve) and 20 V (solid grey curve), and with both ^{235}U and ^{238}U measured using 10^{11} Ω resistors (see Methods and ESI†). The black curve shows the absolute precision limit assuming 100% of ion transmission: *i.e.*, all ions in solution reach the detectors of the instrument.
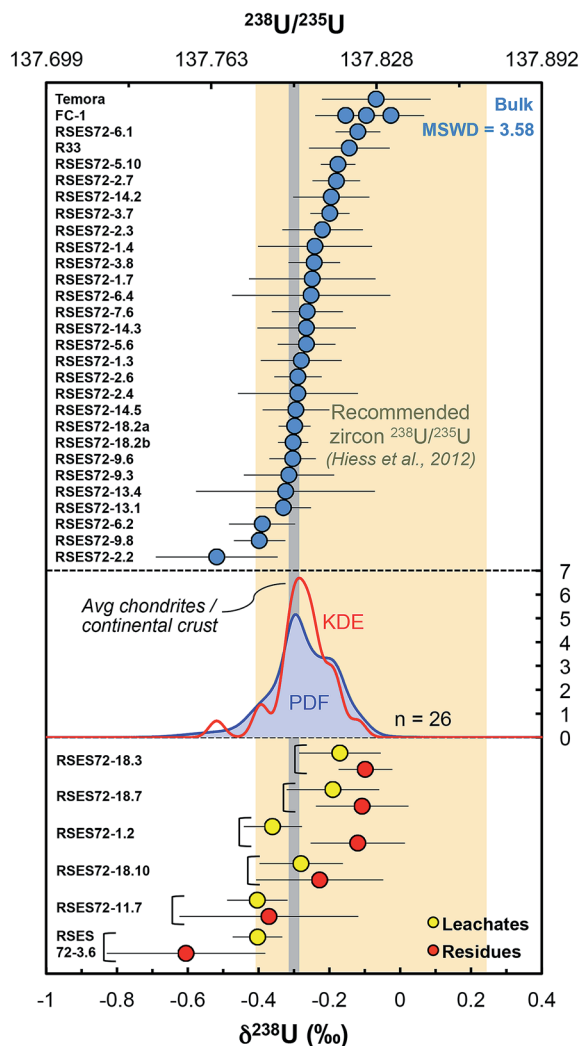
2040 | *J. Anal. At. Spectrom.*, 2019, **34**, 2035–2052

This journal is © The Royal Society of Chemistry 2019

Fig. 5 Single-zircon U isotope data revealing resolvable grain-to-grain variations. Vertical grey band shows the chondritic and continental crust value, while the yellow vertical band shows the recommended $^{238}U/^{235}U$ for use in geochronology. Absolute ratios normalized to $^{238}U/^{235}U = 137.837$ for CRM-112a (ref. 36). The Probability Density Function (PDF, blue curve) and the optimized bandwidth Kernel Density Estimator (KDE, red curve) of the Jack Hills zircons are shown. Leachates (yellow circles) and residues (red circles) from chemical abrasion suggest preferential mobilization of ^{235}U during strong acid attack. The high MSWD (=3.58) for the Jack Hills zircons indicates that these samples are isotopically heterogeneous. The PDF/KDE of the Jack Hills zircons is not centered on the recommended $^{238}U/^{235}U$, suggesting that there is variation in the U isotope composition of zircon populations from different localities.

leachate values between $-0.40 \pm 0.07‰$ (RSES72-3.6) and $-0.17 \pm 0.12‰$ (RSES72-18.3), and residue values between $-0.60 \pm 0.22‰$ (RSES72-3.6) and $-0.10 \pm 0.08‰$ (RSES72-18.3). Less than 20% of the total sample U is released during the HCl and HNO_3 pre-cleaning steps, indicating a small, yet non-negligible potential contribution from iron oxides, secondary alteration products and adsorbed U (Table S1†), highlighting the need for cleaning or chemically abrading the grains before dissolution for U isotope measurements. For five of the six chemically

abraded samples, leachates and residues have indistinguishable $\delta^{238}U$ (within uncertainties), yet, taken at face value, four of these samples show lower $\delta^{238}U$ in the leachates relative to their residue counterpart. For one sample (RSES72-1.2) the leachate ($\delta^{238}U = -0.36 \pm 0.08‰$) is clearly ^{235}U depleted compared to the residue ($\delta^{238}U = -0.12 \pm 0.13‰$), in agreement with pooled zircons data and the suggestion that aggressive acid attacks may preferentially mobilize ^{235}U over ^{238}U (ref. 9 and 12).

6. Discussion

6.1 No evidence for widespread Oklo-type reactors in the early Earth

Under the right conditions, U-rich deposits formed before ∼1.8 Ga, when natural ^{235}U abundance was >∼3%, could have reached criticality. This is particularly true in the Hadean, as ^{235}U abundance was >17%, and the case has been made that a CFF-Xe (CFF = Chemically Fractionated Fission) component, produced by such nuclear reactors, could be present in Earth's atmosphere and explain its Xe isotopic anomalies.[38] Yet, in addition to high ^{235}U abundance, the conditions required for self-sustained neutron-induced ^{235}U fission are non-trivial to meet: (i) a high enough U concentration (∼>10–20 wt% in the Hadean) in a sediment layer of at least 50–100 cm of thickness,[14,39] (ii) the presence of a neutron flux moderator (e.g., water) and sufficient porosity for water circulation (10–20%), and (iii) no significant amount of neutron absorbing elements (e.g., REEs).[40] Our single-zircon $^{238}U/^{235}U$ measurements provide a way to directly test for the possible existence of Oklo-type reactors in the early Earth.

The $^{238}U/^{235}U$ of the 31 Jack Hills zircons cover a range of ∼0.50‰, with the lightest and heaviest samples displaying $\delta^{238}U$ values of $-0.60 \pm 0.22‰$ (RSES72-3.6R) and $-0.12 \pm 0.06‰$ (RSES72-6.1), respectively. This distribution is similar to that of younger igneous rocks, which ranges from -0.50 to $+0.17‰$ (see compilation in ref. 16), and is centered on the chondritic value of $-0.31 \pm 0.29‰$ (2SD, ref. 41). Therefore, our zircon data shows no evidence of ^{235}U burn-up such as the high $\delta^{238}U$ values of +24 to +475‰ documented in the Oklo reactor zones.[15] Moreover, the range of $\delta^{238}U$ values in Hadean/Archean zircons is ∼10× smaller than the ∼6.2‰ range observed in uraninites (UO_2) and younger U ore deposits (see compilation in ref. 16), whose compositions are primarily controlled by redox processes leading to ^{238}U enrichments of up to ∼2‰ in the reduced/mineralized phases. In principle, the 0.50‰ spread in $^{238}U/^{235}U$ in early Earth zircons could thus be explained by minor contributions from natural reactor material (<1% of the U in the grains) and/or incorporation of some amount of sediments whose composition were affected by redox processes (∼25% of the U in the grains). Both scenarii are unlikely because Jack Hills zircons formed before oxidative conditions could solubilize U in water as U^{VI} (ref. 29), therefore precluding redox driven U isotope fractionation in surface environments and preventing oxidative mobilization and accumulation of U in sediments to the wt% levels required for self-sustained neutron-induced ^{235}U fission. A scenario of weathering-transport-sedimentation and tidal sorting of uraninite has, however,

been proposed as a way to produce U-rich sediments capable of reaching criticality.[14,42] Even in this framework, the fact that the range of $\delta^{238}U$ values measured in early Earth zircons is centered on the chondritic value argues against any contribution from sources with high $^{238}U/^{235}U$ (*e.g.*, nuclear reactor material or mineralized ore sediments). As such, our data provides no evidence for the widespread existence of Oklo-type reactors in the Hadean/Archean, at least within the basin sampled by the Jack Hills conglomerate. This casts some doubts on the idea that CFF-Xe could be present in Earth's atmosphere. Analysis of grains from other localities will be necessary to test these hypotheses over a larger geographic scale.

6.2 Potential sources of U isotope variations in single-zircons

As discussed above, the spread in $\delta^{238}U$ values of Jack Hills zircon crystals is unlikely to stem from U incorporation from natural nuclear reactors and/or ^{238}U enriched sediments (*i.e.*, source effects). Below we consider the potential mechanisms that could lead to U isotope fractionation during magmatic processes, and discuss them in the light of the available data.

According to the theory of stable isotope fractionation (review in ref. 43) mass-dependent isotopic effects during equilibrium isotope exchange reactions vary with the temperature of equilibration ($\propto 1/T^2$), as well as the oxidation state and bonding environment (or speciation) of the element being exchanged. Typically, heavy isotopes concentrate where coordination numbers are low, bond distances short and valence is high (*i.e.*, stiffest bonds). For U, another equilibrium isotope effect exists: a mass-independent but volume-dependent effect called Nuclear Field Shift (NFS), which stems from differences in the electron density at the nucleus of the two isotopes.[19] The NFS scales as $1/T$, occurs during isotope exchange reactions

between reduced and oxidized U phases, and results in isotope fractionations $3\times$ larger than, and of direction opposite to, the vibrational mass-dependent effect.[19,44] Changes in the bonding environment, coordination number and/or valence of U during incorporation into minerals could thus lead to $^{238}U/^{235}U$ variations during magmatic differentiation. This hypothesis is consistent with the ^{238}U excesses of 4.8‰ in pooled titanites relative to pooled zircons in the Fish Canyon Tuff sample,[9] the ~0.30‰ variability in multi-grain dissolutions of coexisting phases from single samples (*i.e.*, zircons *vs.* apatite),[9,12] and the ~0.20‰ variations among angrite meteorites that correlate with independent tracers of magmatic differentiation (*e.g.*, REE patterns, mineral abundances).[20] Because individual zircons from single igneous rock samples can form over protracted periods of magmatic fractional crystallization,[45,46] they are thus likely to record changes in $\delta^{238}U$ of the evolving magma, whether or not the fractionation is due to zircon crystallization itself.

We review the available data on U bonding environment and valence in silicate melts and minerals to determine the mechanisms likely to fractionate U isotopes. In silicate melts, three U oxidation states can coexist (U^{IV}, U^{V}, U^{VI}), depending on the melt's oxygen fugacity (fO_2)[47] and alkalinity (ref. 48 and references therein). Under the conditions relevant to most magmatic settings (~QFM buffer), including the Jack Hills zircons (*i.e.*, between IW and QFM buffer[49]), U^{IV} is the dominant species, with U^{V} representing <10% of the total U below QFM−1 and up to 40% of the total U at QFM+0.2 (ref. 47). Structure (EXAFS) spectroscopy of silicate glasses indicates that U^{IV} and U^{V} occur in 6-fold coordination sites, with slightly different mean U–O distances of, respectively, 2.26–2.29 Å and 2.19–2.24 Å. In contrast, U^{VI}, present only under highly oxidizing conditions (>QFM+4), occurs in uranyl groups with two axial oxygens at
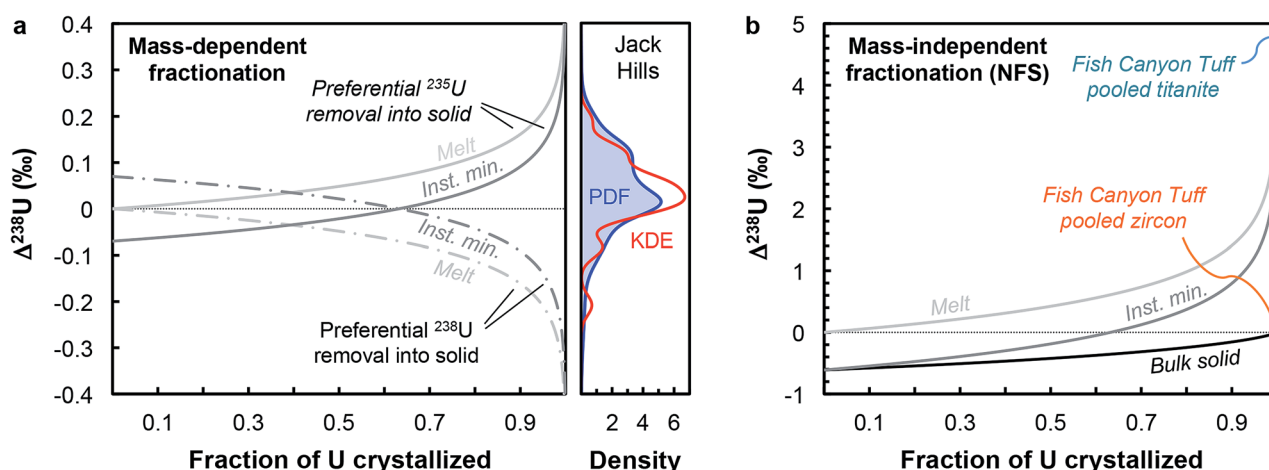

Fig. 6 (a) Melt and instantaneous solid (minerals) U isotope composition evolution during a Rayleigh distillation, as a function of the fraction of U removed from the melt. Two pairs of curves are shown illustrating preferential incorporation of ^{235}U (solid curves) and ^{238}U (dashed curves) into the crystallizing phase. The absolute magnitude of the $\Delta_{mineral-melt}$ fractionation factor is 0.07‰ (expected value for vibrational mass-dependent fractionation effects at 850 °C, see text for details). This small mass-dependent effect can explain the entire spread of $^{238}U/^{235}U$ values in the Jack Hills zircons (see density distribution curves). (b) Same as (a), with addition of the bulk solid evolution curve, but using a $\Delta_{mineral-melt}$ fractionation factor of −0.61‰ (expected value for NFS effects at 850 °C). The 4.8‰ offset between pooled titanite and pooled zircons in the Fish Canyon Tuff sample (data from ref. 9) suggests a redox change during U incorporation into zircons (and/or other accessory phases) in oxidizing silicate melts.

~1.77–1.85 Å, and four to five equatorial oxygens at ~2.21–2.25 Å (ref. 48). Due to its large radius (~0.89 Å) and charge (4+ or more), U is incompatible during magmatic differentiation until minerals capable of accommodating this large cation start crystallizing: *e.g.*, zircon, baddeleyite, titanite, monazite, apatite, biotite, xenotime, allanite.[48] While only limited mineral spectroscopic data is currently available (review in ref. 50), U seems to be predominantly incorporated as U^{IV} in large cation sites in the aforementioned minerals. In zircons, U is thought to be hosted in the large Zr site as U^{IV} (ref. 48 and 51), although some amount of U^{V} has been observed in some natural zircons.[52] The coordination of U in zircons is unclear and both 6-fold[51] and 8-fold[48] have been proposed. In titanite, U^{IV} is incorporated in the 7-coordinated Ca^{II} site *via* coupled substitution of Mg^{II} into the Ti^{IV} site.[53] Although no spectroscopic data is available, monazite is also likely to uptake U^{IV} as it incorporates Th,[54] which is tetravalent only. To our knowledge, there are no data on U bond length or coordination numbers in these phases. Therefore, under the conditions prevailing in most terrestrial magmatic settings (<~QFM), no redox changes are expected to occur during uptake of U from the magma into accessory minerals, and thus changes in the coordination number of U and/or the U–O bond length are the most likely driver of U isotopic fractionation.

Although U isotopic fractionation factors between accessory minerals and silicate liquids remain unknown, resolvable $\delta^{238}U$ differences between accessory phases from the same sample (*e.g.*, zircon *vs.* titanite or apatite[9,12]) indicate that U incorporation in at least one of these minerals is accompanied by a non-zero isotope fractionation at magmatic temperatures. The magnitude of NFS and vibrational mass-dependent U isotopes effects in magmatic settings can, to first-order, be estimated using the temperature dependent expression from Fujii *et al.*[44]: $\varepsilon = 0.69/T - 82/T^2$, where ε is the isotope fractionation factor between U^{IV} and U^{VI} during electron exchange, and T is the temperature in K. At the onset of zircon crystallization (~850 °C, ref. 55), NFS effects would lead to large isotopic fractionation of ~+0.61‰, whereas mass-dependent vibrational effects would result in opposite and more subdued fractionation of ~−0.07‰. By the end of magma crystallization (at ~700 °C), NFS and mass-dependent effects will have increased to, respectively, +0.71‰ and −0.09‰. Distillation effects would result in larger $\delta^{238}U$ variations. In the simplest scenario, assuming that zircon is the only U host phase crystallizing and using the smaller fractionation factors expected at 850 °C, a Rayleigh distillation during fractional crystallization driven by NFS effects would results in a spread of $\delta^{238}U$ values from +0.61‰ to −1.83‰ (at 95% U removal) around the bulk sample value, whereas the same Rayleigh distillation driven by mass-dependent effects would produce variations between −0.07‰ and +0.22‰ around the bulk value (Fig. 6a). In reality, other phases also uptake U, from pyroxenes to late stage forming phases such as titanite, apatite or monazite, all of which can potentially fractionate U isotopes to different degrees depending on the bonding environment and valence of U in their crystal structure. Nonetheless, this simplified scenario is instructive as it reveals that even the small (~0.07‰)

equilibrium mass-dependent U isotope effects expected at 850 °C can explain the entire spread of $^{238}U/^{235}U$ observed in the Jack Hills zircons (Fig. 6a). Without whole-rock and single-zircon data from the same sample, we cannot definitely conclude as to the direction or magnitude of the $\Delta_{zircon\text{-}melt}$ fractionation factor under the conditions (*e.g.*, redox, *T*) relevant to early Earth zircons, and more work will be needed to constrain this value.
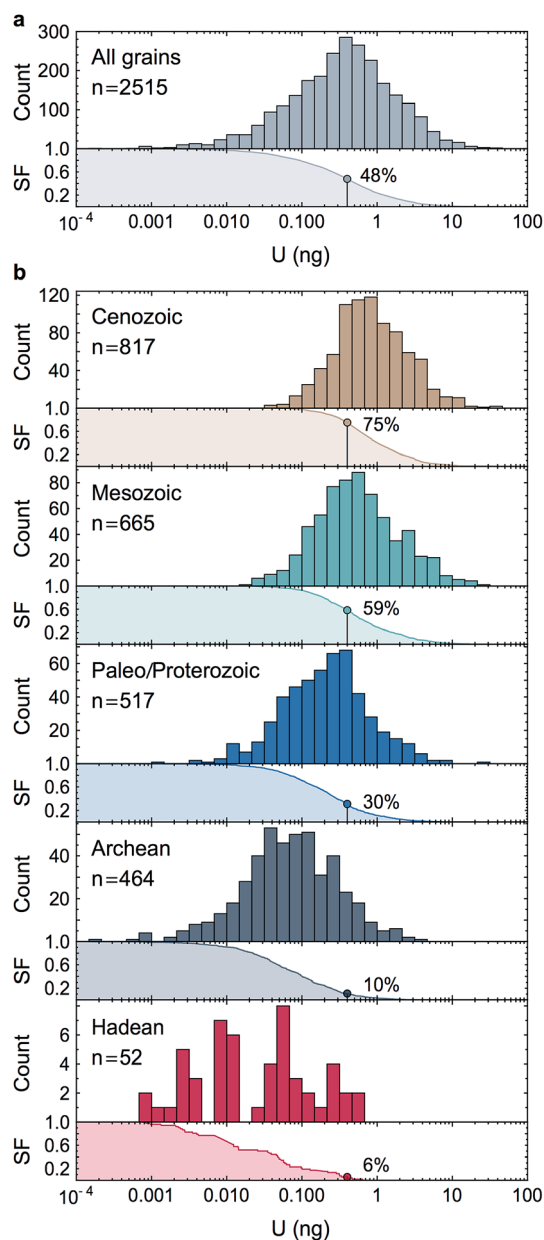

Fig. 7 Histograms and associated survival functions of post chemical abrasion U mass (in ng) recovered from 2515 individual zircon crystals analyzed in recent high-precision geochronology studies (data from ref. 23, 24, 35, 66, 67 and 70–94). (a) All data, (b), data shown by geological time periods. For each panel, the % of grains with more than 0.4 ng of U is shown on the survival function. The decrease in U content with increasing age is an artifact due to the chemical abrasion treatment. Indeed, radiation damages on the crystal lattice are more extensive in older zircons, resulting in greater proportion of the grain being leached away during the chemical abrasion step.

In contrast, the offset in $^{238}U/^{235}U$ between pooled titanite and pooled zircons observed in Fish Canyon Tuff sample[9] provides insight into the mechanisms of U isotope fractionation in magmatic settings under oxidizing conditions ($\sim$QFM+2, ref. 56), and suggests preferential incorporation of ^{235}U in zircons, or some of the other accessory phases crystallizing before titanite (*e.g.*, monazite, apatite). Indeed, the large (4.8‰) ^{238}U excess in titanite cannot be explained solely by a NFS effect during U incorporation into titanite, which at $\sim$850 °C can only produce ^{238}U excesses 0.61‰ above the bulk rock value (which we assume is represented by the pooled zircon value, for lack of bulk rock data). As titanite is a late forming phase,[57] the large ^{238}U excess it records implies that one (or several) of the accessory phases crystallizing before titanite preferentially incorporated ^{235}U, driving the melt composition towards higher $\delta^{238}U$ values during differentiation. Assuming that the $\Delta_{\text{titanite-melt}}$ is negligible, a 4.8‰ excess in the residual melt would require formation of titanite after more than 99% of U removal into other phases associated with a NFS $\Delta_{\text{solid-melt}}$ of -0.61‰ (Fig. 6b), suggesting a redox change during U incorporation into zircons (and/or other accessory phases) in oxidizing silicate melts.

At this writing, the available $\delta^{238}U$ data from different phases within a single sample is too limited to allow systematic trends to be identified. For instance, Hiess *et al.*[9] reported $\delta^{238}U$ values 0.23 ± 0.06‰ lower in apatite than zircon of the Mud Tank carbonatite, whereas Livermore *et al.*[12] reported values up to 0.30‰ higher in apatite than in zircons in leucogabbro and orthogneiss from Labrador. These differences could be explained in at least two ways: (1) by different crystallization times of apatite from a magma of evolving U isotope composition; or (2) by different U coordination environment in carbonatite and silicate melts, leading to opposite equilibrium fractionation in these phases during fractional crystallization. Single-grain U isotope analysis will allow investigations of these questions through quantification of mineral-melt fractionation factors, and the extent of $\delta^{238}U$ variability within a mineral type for any given sample.

6.3 A shift in global zircon $^{238}U/^{235}U$ after the Paleo-archean?

Multi-grain zircon dissolution data,[9,12] which include samples spanning Earth's post-Eo-Archean history, are not centered on the chondritic (-0.31 ± 0.29‰, ref. 41) or bulk continental crust value (-0.29 ± 0.03‰, ref. 16), but are displaced toward higher $\delta^{238}U$ values by $\sim$0.20‰ (Fig. 5). In contrast, the Jack Hills zircons $\delta^{238}U$ distribution is indistinguishable from that of chondrites and the bulk continental crust. Taken at face value, this suggests an increase in $^{238}U/^{235}U$ in (some) zircon populations sometime after the Eo- to Paleo-archean transition. Such increase in $^{238}U/^{235}U$ could be the result of either (1) the influence of source materials with higher $\delta^{238}U$ in younger rocks, or (2) a change in mantle redox conditions sometime after the Eo-Archean, allowing the expression of a stronger zircon-melt U isotope fractionation than those observed in older zircons. More work on Hadean/Archean zircons will be

necessary to confirm the statistical significance of the $\delta^{238}U$ offset relative to younger zircons.

6.4 Practical relevance of single grain analyses for U–Pb and Pb–Pb geochronology

Owing to analytical advances, sources of uncertainty that were once dominant (*e.g.*, procedural blank, instrumental mass fractionation, Pb-isotope counting statistics) no longer represent a major impediment for high precision U–Pb and Pb–Pb geochronology. State-of-the-art measurements[58,59] using CA-ID-TIMS (chemical abrasion-isotope dilution-thermal ionization mass spectrometry[10,30]) can now attain single-zircon U–Pb date precisions on the order of 0.2‰. Although laboratory blank Pb isotope composition and U-series disequilibrium remain a main limitation for high-precision $^{206}Pb/^{238}U$ dating of Phanerozoic zircons,[60] the accuracy with which geological events in the Proterozoic and earlier rock/mineral record can be determined is now significantly limited by how precisely and accurately the sample $^{238}U/^{235}U$ is known. Single-zircon $^{238}U/^{235}U$ measurements have been theoretically recognized as a way to refine U–Pb and Pb–Pb geochronology, but the small U mass harvested from individual zircons has led to claims that only limited, if any, improvements could be gained from such measurements.[10–12] Here, we consider these claims in the light of our data.

For single-zircon $^{238}U/^{235}U$ analyses, uncertainties vary as a function of the amount of U measured (Fig. 4b) and are often limited by counting statistics. Nevertheless, the ± 0.25‰ external reproducibility uncertainty (2SE) obtained here on U loads of only 2 ng is still 25% smaller than the ± 0.33‰ uncertainty associated with the 'recommended $^{238}U/^{235}U$ value' that is widely used for U–Pb geochronology[9] (grey band, Fig. 4b). Moreover, by measuring ^{235}U on a 10^{12} Ω instead of a 10^{11} Ω amplifier, precision better than 0.30‰ can theoretically be achieved for U loads as low as 0.4–0.5 ng (see Section 6.6). To determine if these U-mass limits are an impediment for application of single-zircon $^{238}U/^{235}U$ analysis to high-precision geochronology, literature data from 2515 individual zircon crystals dated by CA-ID-TIMS at the MIT and Princeton University labs were compiled (Fig. 7). The compilation includes grains covering Earth's history and shows that the typical U mass recovered from chemically abraded zircons ranges from 0.01 to 10 ng. Contrary to the prevailing notion that chemical abrasion results in insufficient amounts of U for precise $^{238}U/^{235}U$ determination in routine U–Pb geochronology analyses,[9–12] the data reveal that 48% of the zircons in those studies yielded more than 0.4 ng of U, and 24% yield more than 1 ng of U. Therefore, virtually every other zircon dated by the CA-ID-TIMS method would be amenable to single-grain U isotope measurements.

6.5 Implications for U–Pb and Pb–Pb geochronology

Below we show how single-grain U isotope measurements would yield more accurate, and in many instances more precise, high-precision Pb–Pb and U–Pb dates than those calculated using a 'recommended' $^{238}U/^{235}U$ ratio.[9,12] To the exception of the section discussing chemically abraded zircons, the general chronological considerations below directly apply to all U–Pb
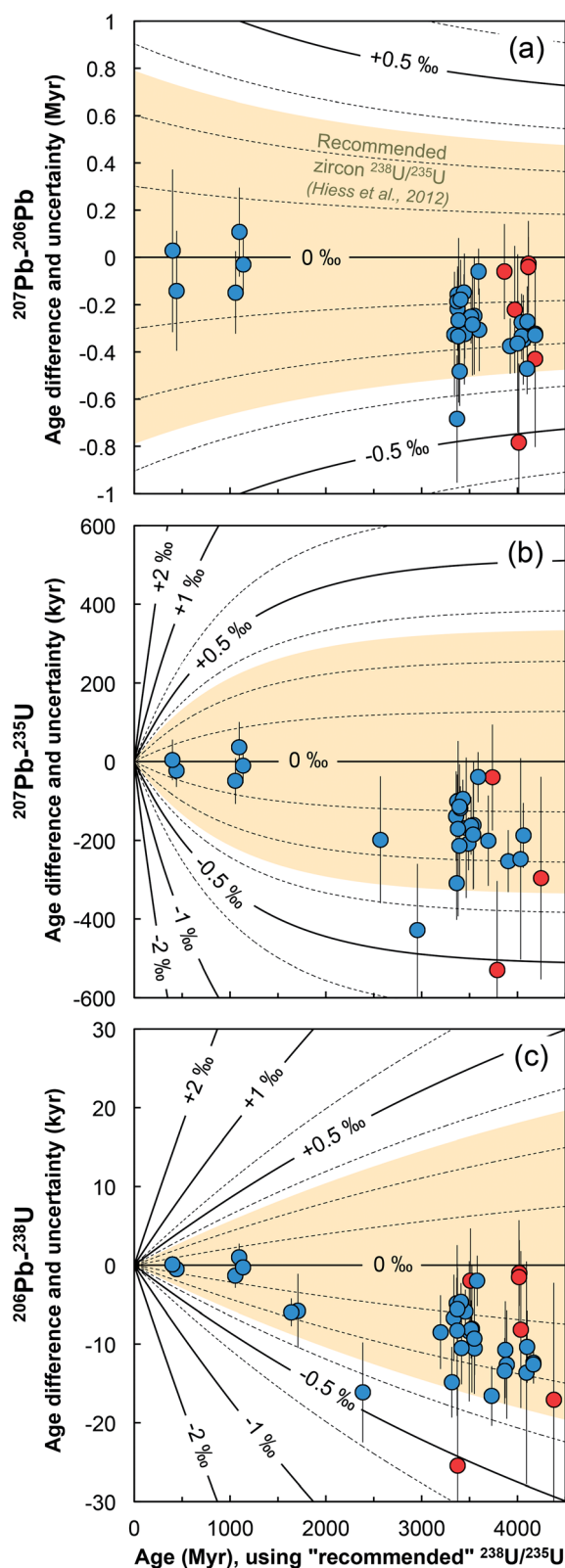
2044 | *J. Anal. At. Spectrom.*, 2019, 34, 2035–2052

This journal is © The Royal Society of Chemistry 2019

Fig. 8 Age corrections for the (a) $^{207}Pb-^{206}Pb$, (b) $^{207}Pb-^{235}U$ and (c) $^{206}Pb-^{238}U$ ages of the zircons measured in this work (blue = bulk grain, red = chemical abrasion residue) stemming from the difference between the recommended $^{238}U/^{235}U$ from ref. 9 and the ratio measured in each grain. Lines of equal ΔU values (ΔU = [$^{238}U/^{235}U_{sample}/^{238}U/^{235}U_{Hiess}$ − 1] × 1000, in ‰) are shown and were calculated using eqn (A.3), (A.4), and (A.5).

geochronology, including other U-rich accessory phases such as baddeleyite,[61] or titanite.[62,63]

6.5.1 In a single grain. The typical accuracy and precision improvements brought by single-zircon $^{238}U/^{235}U$ measurements are best shown as age offsets resulting from the difference between the measured and assumed $^{238}U/^{235}U$ (Fig. 8). Although U–Pb dates should theoretically be independent of the $^{238}U/^{235}U$ ratio, they are also affected because ID-TIMS analyses are most commonly made using $^{233}U-^{235}U$ mixed spikes (e.g., ET-535 and ET-2535; ref. 10), which require knowledge of the sample $^{238}U/^{235}U$ to correct for U mass fractionation during sample preparation and analysis.[64,65] Moreover, due to the low thermal ionization efficiency of U metal, isotopic measurements by ID-TIMS are typically made as oxides.[10] This requires that uncertainties in the effective isotopic composition of oxygen be taken into account. While some methods exist to minimize the contribution of U-oxide correction uncertainties,[10,59] direct measurement of single-zircon $^{238}U/^{235}U$ by MC-ICPMS removes this source of uncertainty altogether.

To further illustrate the impact that single-zircon $^{238}U/^{235}U$ analysis can have on high-precision Pb–Pb and U–Pb age determinations, we use data from two geologically important samples: a 1.09 Ga Midcontinent Rift zircon[66] and a 3.97 Ga lunar zircon.[67] While Midcontinent Rift zircon dates have been used to constrain the rates of plate motions in the past, lunar zircons provide the most direct constraint on the age of the Moon. Substituting the median $^{238}U/^{235}U$ uncertainty of our

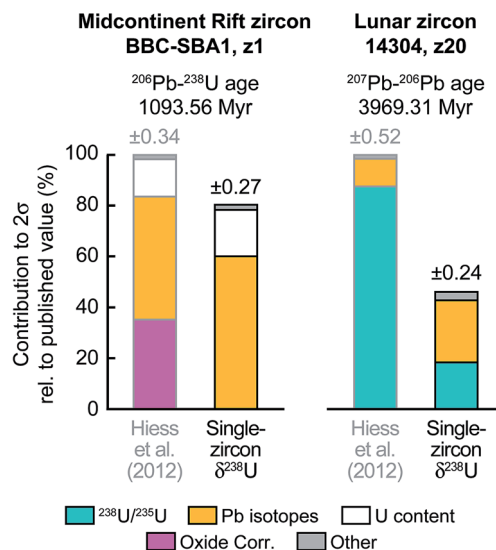**Fig. 9** Contribution of the different sources of uncertainty to the high-precision $^{206}U-^{238}Pb$ age of a 1.09 Ga Midcontinent rift zircon[66] (sample BBC-SBA1, fraction z1) and the $^{207}Pb-^{206}Pb$ age of a 3.97 Ga lunar zircon[67] (sample 14 304, fraction z20). $^{206}U-^{238}Pb$ and $^{207}Pb-^{206}Pb$ dates are typically reported for events younger and older, respectively, than ~1.5 Ga. For each sample the published errors calculated using the recommended $^{238}U/^{235}U$ from ref. 9 are compared to the errors that would be achieved if a single-zircon U isotope measurement with precision of ±0.10‰ had been performed instead. Details of error contribution on all Pb–Pb and U–Pb ages are shown in ESI Fig. S1.†

This journal is © The Royal Society of Chemistry 2019

J. Anal. At. Spectrom., 2019, **34**, 2035–2052 | **2045**

measurements (*i.e.*, $\pm$ 0.10‰) in place of the $\pm$ 0.33‰ uncertainty of the recommended value from Hiess *et al.*,[9] we estimate that, in addition to an increase in accuracy, ^{207}Pb–^{206}Pb dates would become 23 to 54% more precise (Fig. 9 and S1†). Provided laboratory blank and instrumental Pb mass fractionation are not the main sources of uncertainty, removal of the U-oxide correction uncertainty through MC-ICP-MS ^{238}U/^{235}U measurement could improve the typical precision of ^{206}Pb–^{238}U and ^{207}Pb–^{235}U dates by 6 to 22% (Fig. 9 and S1†).

6.5.2 In a grain population. To achieve higher precision and provide stronger temporal constraints, geochronological studies typically report the weighted mean age of ~15–20 zircon grains coming from the same sample. Since it is assumed that grains of similar apparent age formed at the same time, it is common practice to reject "outlier" grains based on their ages alone, so as to achieve a weighted mean

with near unit MSWD. This practice implicitly assumes that all grains have the same ^{238}U/^{235}U. A Monte-Carlo analysis (ESI†) exploring the effect of U isotope variability on the accuracy of the weighted mean of 20 co-genetic zircon grains reveals statistically significant effects on both ^{207}Pb–^{206}Pb and ^{207}Pb–^{235}U ages as soon as individual grain age precisions better than 0.05 to 0.10% are achieved (Fig. 10). This implies that at such high precision, and in the absence of single-zircon U isotope data, rejecting grains based solely on their apparent ages to achieve a unit MSWD does not ensure that the rejected grains are true outliers. In such scenarii, single-zircon ^{238}U/^{235}U analyses will allow to better assess whether grains belong to the same population, and to calculate more meaningful and accurate weighted mean ages. Given that decay constants errors almost completely cancel out when considering age intervals,[20] the improvements in precision and
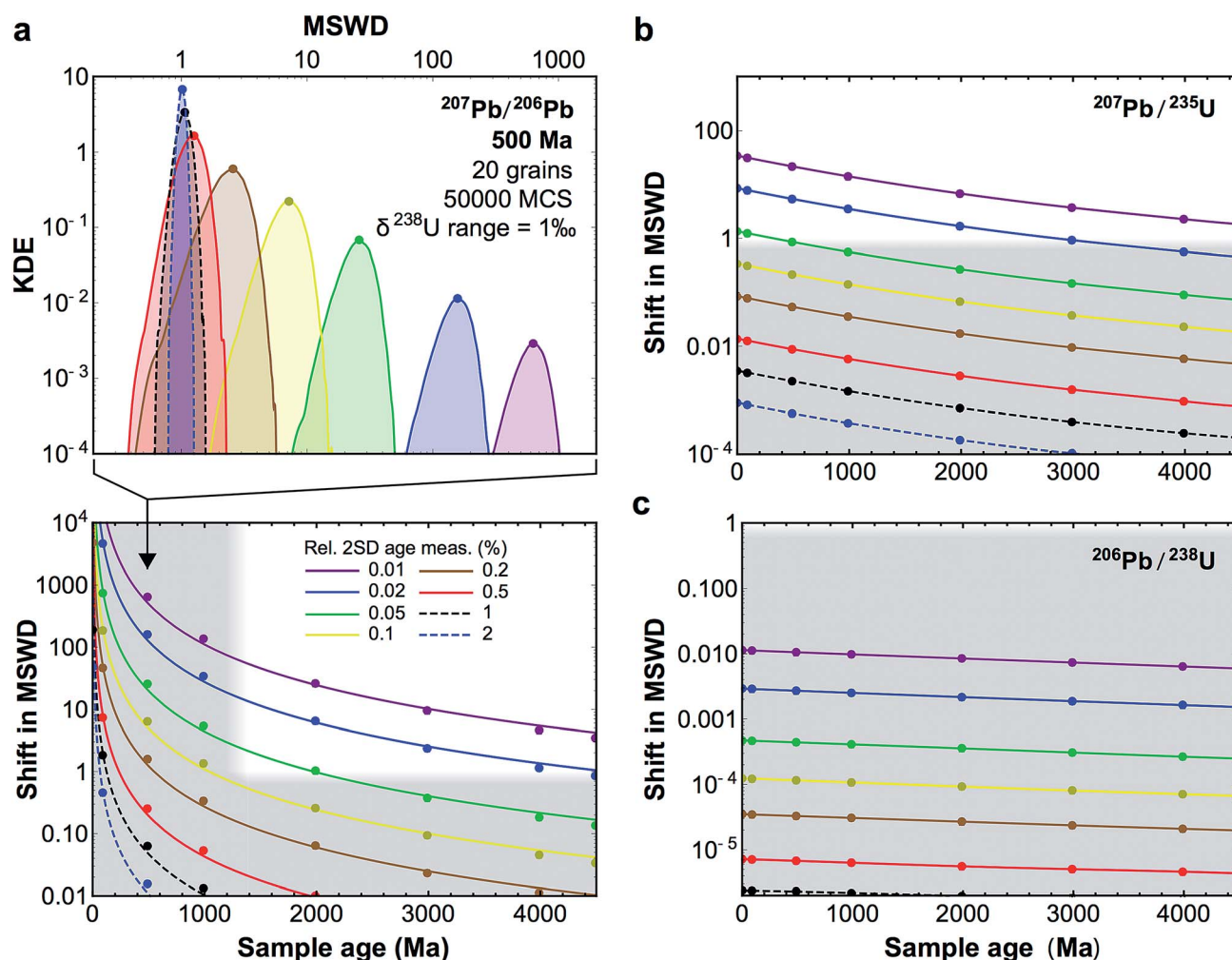

Fig. 10 (a, top-panel) Example of KDE of the U-corrected MSWD of the weighted mean age calculated for 500 Ma zircons (20 grains), for relative precision on the age measurement of individual grains between 2 and 0.01% (see legend bottom panel). The Monte-Carlo analysis used 50 000 simulations (MCS) and δ^{238}U values were randomly picked within a uniform distribution of width 1‰, centered on the 'recommended' value from ref. 9. For simplicity, and to be conservative, age uncertainties are kept constant before and after age correction: *i.e.*, only the improvement in accuracy is evaluated. (a, bottom-panel) Median shift in MSWD of the weighted mean ^{207}Pb/^{206}Pb age of 20 zircon grains resulting from U-based age corrections. Grey areas denote statistically insignificant shifts (horizontal band), and ages for which ^{206}Pb–^{238}U ages are preferred to ^{207}Pb–^{206}Pb ages (which are too imprecise, vertical band). (b and c) Same as bottom-panel a, but for ^{207}Pb–^{235}U and ^{206}Pb–^{238}U ages, respectively.

2046 | *J. Anal. At. Spectrom.*, 2019, **34**, 2035–2052

This journal is © The Royal Society of Chemistry 2019

accuracy achievable through single-zircon $^{238}U/^{235}U$ measurements will provide unprecedented resolution power for establishing the timescales of short-lived events and processes.

6.5.3 $^{206}Pb-^{238}U$ ages. Although $^{238}U/^{235}U$ variations predominantly impact the accuracy of $^{207}Pb-^{235}U$ and $^{207}Pb-^{206}Pb$ dates over $^{206}Pb-^{238}U$ dates (Fig. 8, 10, and ESI†), the existence of extremely fractionated $\delta^{238}U$ values in some zircons (*e.g.*, Table Cape pooled zircon; ^{238}U excess of 3.4‰; ref. 9) means that even $^{206}Pb-^{238}U$ dates will be affected in some rare occasions. For a 250 Ma old zircon, a difference of 3.4‰ between the assumed and actual $^{238}U/^{235}U$ would translate into an age offset of ~15.4 kyr. This offset is similar in magnitude to the extent by which the end-Permian extinction is currently resolved from being an instantaneous event (60 ± 48 kyr; ref. 23). Thus, examination of the rock record at sub-permil age precision, even in Phanerozoic samples,[23,68] will benefit from concomitant measurement of U isotopes for as long as ^{235}U-based spikes are utilized.

6.5.4 Concordance and half-lives. Uranium isotopic analyses will also prove useful in assessing U–Pb dates concordance. For CA-ID-TIMS U–Pb dates, small degrees of discordance are mainly interpreted as the result of disequilibrium incorporation of intermediate daughter products in a sample,[45,68] and/or systematic errors in the U decay constants.[27,31] Disequilibrium effects are only significant for the longest-lived nuclides, ^{230}Th ($t_{1/2}$ = 75.4 ky) and ^{231}Pa ($t_{1/2}$ = 32.76 ky), and affect, respectively, $^{206}Pb-^{238}U$ and $^{207}Pb-^{235}U$ dates. Given the strong sensitivity of $^{207}Pb-^{235}U$ dates to U isotope variations, single-zircon $^{238}U/^{235}U$ measurements will (i) help resolve the contributions of intermediate daughter disequilibrium to the discordance of U–Pb dates observed in some samples[45,68]

(Fig. 11), and (ii) allow a proper re-evaluation of the accuracy of U decay constants, for which revisions have only been proposed based on non-U-corrected U–Pb ages[27,31] or U–Pb ages calculated using pooled zircon data.[9] This latter key advantage will enable a finer-scale calibration of other radio-chronometers (*e.g.*, Ar–Ar) against the Pb clock.

6.6 Current limitations and future improvements

Some zircons will be either too small, too radiation damaged, or too U-poor to yield sufficient U amounts for high-precision single-zircon U analysis. Taking a fiducial amount of U of 0.4 ng (see below), we estimate (Fig. 7) that ~50% of zircons will contain too little U to allow direct $^{238}U/^{235}U$ measurement with current methodologies. The precision achieved in this study is at the theoretical level of MC-ICPMS counting statistics (Fig. 4b) but only ~2.5% of the atoms in the solution make it to the detector. A recent study showed that up to 5% efficiency for U was achievable using cavity source TIMS.[69] There is thus ample room for improvement as the transmission of mass spectrometers continues to improve (black curve on Fig. 4b shows absolute precision limit: 100% ion transmission). In cases where U contents remain too low, measurement of small pooled fractions of co-genetic zircons (*e.g.*, 2 to 5 grains) is the only way to obtain useful estimates approaching the true sample $^{238}U/^{235}U$ variability, for high-precision Pb–Pb and U–Pb chronology.

The method presented here is by no means fully optimized and significant improvements would help make single-zircon U isotope measurements more routine. In particular, exploration of the parameter space relevant to measurement precision using eqn (2) reveals that using higher spiking ratios and
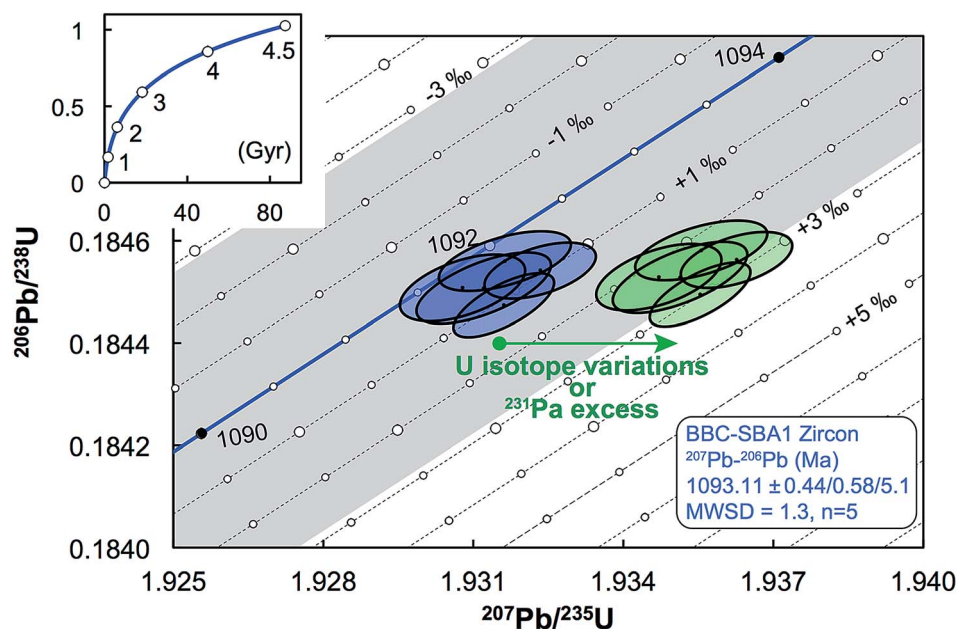

Fig. 11 Concordia diagram, with error envelope due to the uncertainty in U half-lives (grey), showing the effect of a difference between actual and assumed $^{238}U/^{235}U$ of the sample. Lines of equal ΔU values are 1‰ apart and were calculated using eqn (A.1) and (A.2). Also shown are the data for five zircons from the Midcontinent rift sample BBC–SBA166 (blue).[66] Excess of ^{231}Pa and U isotope variations both result in horizontal displacement of the data in a concordia diagram (green), and as such, disequilibrium of intermediate decay products can only be properly assessed if single-zircon U isotope measurements are performed. Half-lives and their uncertainties from ref. 95.

amplifiers equipped with 10^{12} and/or 10^{13} Ω resistors could significantly improve measurement precision for small U loads (<2 ng U, Fig. 12).

6.6.1. Increasing spiking ratio. Regardless of the amplifier setup and for sample loads as low as 0.4 ng of U, uncertainties plateau beyond a spiking level, U_{Sp}/U_{Smp}, of ~8–10% (Fig. 12). This spiking ratio is higher than the value of 3% used in the present work, and should supersede it for future work on low U amounts. Increasing the spiking level will increase the spike contribution to the ^{235}U and ^{238}U budget, but even at U_{Sp}/U_{Smp} = 10% these contributions remain minimal (0.3‰ and 0.01‰, respectively). As long as the sample and bracketing standards have similar spiking levels, no systematic bias will be introduced and measurement uncertainties on the ^{238}U/^{235}U will thus be efficiently minimized. The same is not true for ^{234}U where the spike contribution would reach ~349‰ for U_{Sp}/U_{Smp} = 10%, which would require propagation of the error of the spike ^{234}U abundance onto the final uncertainty of the ^{234}U/^{238}U reported.

6.6.2. Use of high ohmic amplifiers. For a given amount of U analyzed, the achievable uncertainties are lowered by measuring ^{235}U, and to a much lesser extent ^{233}U + ^{236}U on 10^{12} and/or 10^{13} Ω resistors (Fig. 12). Using a U_{Sp}/U_{Smp} of 10%, optimal precisions achievable with modern instrumentation are shown in Fig. 13 as a function of (i) the total U measured (assuming a 10 V signal on ^{238}U), and (ii) the resistance linked to the amplifier used to measure ^{235}U. As can be seen on Fig. 13, measurement precisions improve by more than 0.1‰ on δ^{238}U values for low U amount analyses (below 1 ng of U) when using a 10^{12} to 10^{13} Ω resistor to measure ^{235}U. At such high spiking levels, changing the resistance linked to the amplifier used to measure ^{233}U and ^{236}U from 10^{11} to 10^{13} Ω has virtually no impact on the results. Uncertainties on the order of ±0.30‰ can still be achieved using only 0.4–0.5 ng of U, implying that single-zircon ^{238}U/^{235}U measurement can provide higher precision and accuracy than the currently recommended ^{238}U/^{235}U ratio from ref. 9, even for grains with such low U sample loads.
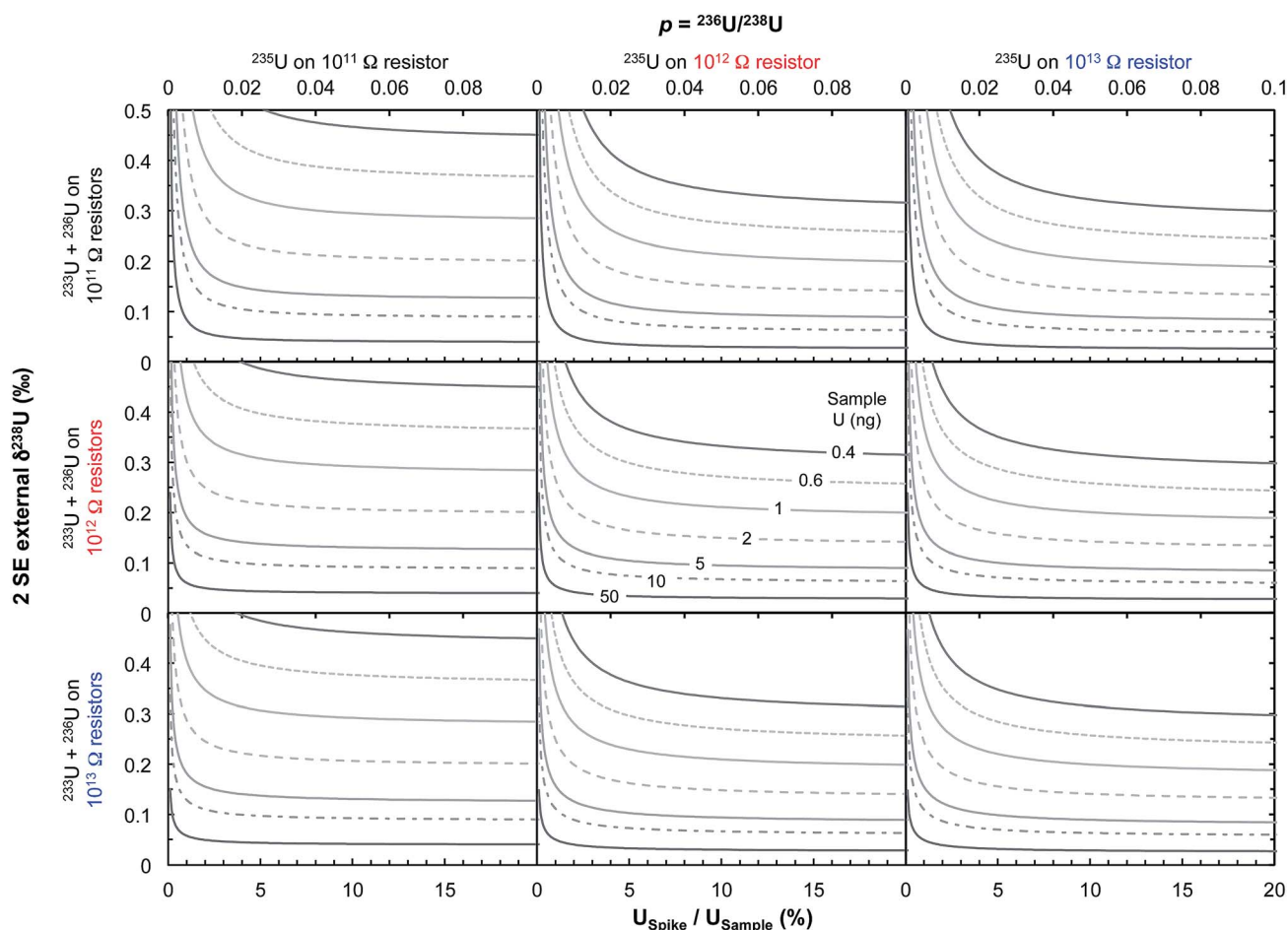

Fig. 12 Theoretical limit on δ^{238}U values uncertainty (2 SE external) achievable on Neptune MC-ICPMS plotted as a function of the sample spiking level (bottom x-axis, U_{Spike}/U_{Sample}; top x-axis, parameter p from eqn (2), which relates the number of ions of ^{236}U and ^{238}U as: $n_6 = p \, n_8$). The various curves represent different amounts of total U measured (in ng). Uncertainties are calculated using eqn (2), assuming ^{238}U is measured at 10 V with a 10^{11} Ω resistor, and each cycle of 4.192 s consumed 0.072 ng of U. Left, center and right panels assume that ^{235}U is measured using, respectively, a 10^{11}, 10^{12} or 10^{13} Ω resistor, with the top, center and bottom row assume that the spike isotopes (^{233}U and ^{236}U) are measured using, respectively, 10^{11}, 10^{12} or 10^{13} Ω resistors, respectively. For small U loads, optimal precision can be achieved using U_{Spike}/U_{Sample} ratio of ~8–10% (where uncertainties plateau) and by measuring ^{235}U in a 10^{12} or 10^{13} Ω resistor.

2048 | *J. Anal. At. Spectrom.*, 2019, **34**, 2035–2052
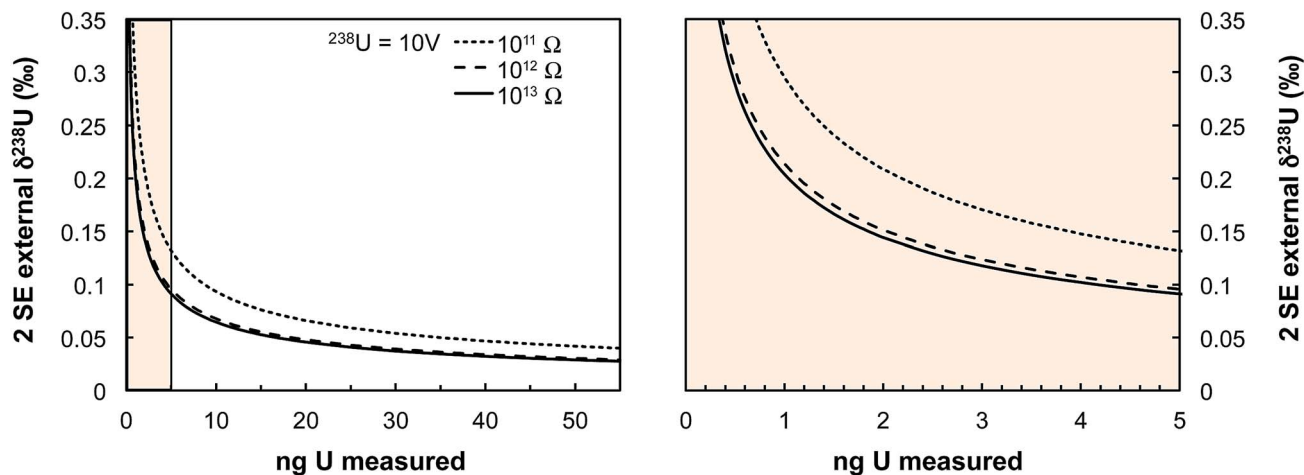
This journal is © The Royal Society of Chemistry 2019

Fig. 13 Theoretical limit on δ^{238}U values uncertainty (2 SE external) achievable on Neptune MC-ICPMS plotted as a function of the amount of U measured (in ng). Uncertainties are calculated using eqn (2) assuming a U_{Sp}/U_{Smp} of 10%, that ^{238}U is measured at 10 V with a 10^{11} Ω resistor, and that each cycle of 4.192 s consumed 0.072 ng of U. The three black curves show the theoretical lower limit achievable when ^{235}U is measured using a 10^{11}, 10^{12} or 10^{13} Ω resistor (see legend). The spike isotopes can be measured with 10^{11}, 10^{12} or 10^{13} Ω resistors without any significant impact on the results given the high spiking level. Even for U sample loads as low as 0.4–0.5 ng, a precision of 0.30‰ is achievable, comparable to the ± 0.33‰ of the recommended ^{238}U/^{235}U value from ref. 9.

6.6.3 Micro-column chemistry. The U purification protocol used here, developed for large sample masses with complex matrices,[16] results in blanks of up to ~0.02 ng, which would be significant for high-precision U–Pb and Pb–Pb dating of loads ~0.4 ng U. Purifying U using the 50 μL AG1-X8 columns typically used in U–Pb geochronology (e.g., ref. 31) would decrease elution volumes, and consequently blanks, by a factor > 250 (from 85 mL to 300 μL), thus streamlining integration of single-zircon ^{238}U/^{235}U measurement into geochronological work.

7. Concluding remarks

As the exact origin of U isotope variations in zircons is unknown, future investigations using extended X-ray absorption fine structure (EXAFS) and/or synchrotron spectroscopy will be needed to address the cruel lack of data on the bonding environment (bond length, coordination number) and valence state of U in minerals. Future works trying to understand the causes of these variations in greater detail could explore potential correlations between ^{238}U/^{235}U ratios and other geochemical and isotopic tracers of magmatic and/or source rock nature and evolution, such as Th/U ratios, oxygen isotopes, initial ^{176}Hf/^{177}Hf ratios, or Ti-thermometry. Through such investigations, which are beyond the scope of this study, single-zircon ^{238}U/^{235}U analysis has the potential of becoming a new tool to probe processes of crustal formation and differentiation, potentially tied to sediment burial or changes in the oxygenation state of the atmosphere-ocean system.

Author contributions

FT, PB, MI and ND initiated the study; FT, PB and MI designed the research; TMH provided the Jack Hills zircons; FT and MI performed the research. FT performed the measurements on ND's and DM's instruments and analyzed the data (including modeling). FT, MI and PB interpreted the data. FT wrote the manuscript with contributions from all co-authors.

Data and materials availability

All data needed to evaluate the conclusions in the paper are present in the paper and/or the ESI.† Additional data related to this paper may be requested from the authors.

Appendix A: shift in concordia space and age corrections

For a given sample, unrecognized U isotope variations will lead to erroneous age calculations[9,16] and shifts in a concordia diagram (Fig. 11), which were quantified using the following analytical formulae (see derivations in the ESI†). Let's consider ΔU, the difference between the actual and assumed U isotope composition of the sample, and defined as: ΔU = $\left(^{238}U/^{235}U_{actual}/^{238}U/^{235}U_{assumed} -1\right) \times 1000$).

Parameters specific to the spike used for the U–Pb measurement will influence the magnitude of these age and concordia offsets. Here we take the example of U–Pb measurements made with the EARTHTIME ET535 tracer (a mixed

^{205}Pb–^{233}U–^{235}U tracer). For a given shift in U isotope composition, the corresponding shifts in the ratio of radiogenic Pb isotope to parent U isotope, ^{206}Pb*/^{238}U and ^{207}Pb*/^{235}U, are respectively noted $\Delta R68$ and $\Delta R75$, and calculated as:

$$\Delta R68 = \frac{(e^{\lambda_{238}t8} - 1)R85m}{400R_U - 1000R85m}\Delta U, \quad (A.1)$$

and

$$\Delta R75 = \frac{(e^{\lambda_{235}t5} - 1)}{1000 - \frac{2500R85m}{R_U}}\Delta U, \quad (A.2)$$

where λ_i is the half-life of isotope i, $R85m$ is the ^{238}U/^{235}U measured in the sample + spike mix, R_U is the assumed ^{238}U/^{235}U of the sample, and $t8$ and $t5$ are the uncorrected ^{206}Pb/^{238}U and ^{207}Pb–^{235}U ages of the sample, respectively (i.e., calculated using the assumed ^{238}U/^{235}U).

Similarly, for a given shift in U isotope composition, the corresponding offsets in ^{207}Pb/^{206}Pb, ^{206}Pb/^{238}U and ^{207}Pb/^{235}U dates, are respectively noted Δt, $\Delta t8$ and $\Delta t5$, and calculated as (see derivations in ESI†):

$$\Delta t = \frac{\Delta U(e^{\lambda_{238}t} - 1)(e^{\lambda_{235}t} - 1)}{1000(\lambda_{238}e^{\lambda_{238}t} - \lambda_{235}e^{\lambda_{235}t} + (\lambda_{235} - \lambda_{238})e^{(\lambda_{235}+\lambda_{238})t})}, \quad (A.3)$$

$$\Delta t8 = \frac{(1 - e^{-\lambda_{238}t8})R85m}{400R_U - 1000R85m}\frac{\Delta U}{\lambda_{238}}, \quad (A.4)$$

$$\Delta t5 = \frac{(1 - e^{-\lambda_{235}t5})}{1000 - \frac{2500R85m}{R_U}}\frac{\Delta U}{\lambda_{235}}. \quad (A.5)$$

Conflicts of interest

Authors declare no competing interests.

Acknowledgements

Notes and references

1 S. A. Bowring and I. S. Williams, Contrib. Mineral. Petrol., 1999, 134, 3–16.

2 T. M. Harrison, Annu. Rev. Earth Planet. Sci., 2009, 37, 479–505.

3 T. M. Harrison, E. A. Bell and P. Boehnke, Rev. Mineral. Geochem., 2017, 83, 329–363.

4 A. Morbidelli, D. Nesvorny, V. Laurenz, S. Marchi, D. C. Rubie, L. Elkins-Tanton, M. Wieczorek and S. Jacobson, Icarus, 2018, 305, 262–276.

5 E. A. Bell and T. M. Harrison, Earth Planet. Sci. Lett., 2013, 364, 1–11.

6 M. T. Rosing, Science, 1999, 283, 674–676.

7 S. J. Mojzsis, G. Arrhenius, K. D. McKeegan, T. M. Harrison, A. P. Nutman and C. R. L. Friend, Nature, 1996, 384, 55–59.

8 J. W. Valley, A. J. Cavosie, T. Ushikubo, D. A. Reinhard, D. F. Lawrence, D. J. Larson, P. H. Clifton, T. F. Kelly, S. A. Wilde, D. E. Moser and M. J. Spicuzza, Nat. Geosci., 2014, 7, 219–223.

9 J. Hiess, D. J. Condon, N. McLean and S. R. Noble, Science, 2012, 335, 1610–1614.

10 D. J. Condon, B. Schoene, N. M. McLean, S. A. Bowring and R. R. Parrish, Geochim. Cosmochim. Acta, 2015, 164, 464–480.

11 N. M. McLean, D. J. Condon, B. Schoene and S. A. Bowring, Geochim. Cosmochim. Acta, 2015, 164, 481–501.

12 B. D. Livermore, J. N. Connelly, F. Moynier and M. Bizzarro, Geochim. Cosmochim. Acta, 2018, 237, 171–183.

13 F. L. H. Tissot, N. Dauphas and L. Grossman, Sci. Adv., 2016, 2(3), e1501400.

14 I. G. Draganic, Z. D. Draganic and D. Altiparmakov, Precambrian Res., 1983, 20, 283–298.

15 J. R. Lancelot, A. Vitrac and C. J. Allegre, Earth Planet. Sci. Lett., 1975, 25, 189–196.

16 F. L. H. Tissot and N. Dauphas, Geochim. Cosmochim. Acta, 2015, 167, 113–143.

17 M. B. Andersen, C. H. Stirling and S. Weyer, Non-Traditional Stable Isotopes, 2017, vol. 82, pp. 799–850.

18 F. Z. Teng, N. Dauphas and J. Watkins, Non-Traditional Stable Isotopes, Mineralogical Society of America, 2017.

19 J. Bigeleisen, J. Am. Chem. Soc., 1996, 118, 3676–3680.

20 F. L. H. Tissot, N. Dauphas and T. L. Grove, Geochim. Cosmochim. Acta, 2017, 213, 593–617.

21 Y. Amelin, A. Kaltenbach, T. Iizuka, C. H. Stirling, T. R. Ireland, M. Petaev and S. B. Jacobsen, Earth Planet. Sci. Lett., 2010, 300, 343–350.

22 T. J. Blackburn, P. E. Olsen, S. A. Bowring, N. M. McLean, D. V. Kent, J. Puffer, G. McHone, E. T. Rasbury and M. Et-Touhami, Science, 2013, 340, 941–945.

23 S. D. Burgess, S. Bowring and S. Z. Shen, Proc. Natl. Acad. Sci. U. S. A., 2014, 111, 3316–3321.

24 B. Schoene, K. M. Samperton, M. P. Eddy, G. Keller, T. Adatte, S. A. Bowring, S. F. R. Khadri and B. Gertsch, Science, 2015, 347, 182–184.

25 J. H. F. L. Davies, A. Marzoli, H. Bertrand, N. Youbi, M. Ernesto and U. Schaltegger, Nat. Commun., 2017, 8, 15596.

26 B. Schoene, M. P. Eddy, K. M. Samperton, C. B. Keller, G. Keller, T. Adatte and S. F. R. Khadri, Science, 2019, 363, 862–866.

27 J. M. Mattinson, Chem. Geol., 2010, 275, 186–198.

28 P. Holden, P. Lanc, T. R. Ireland, T. M. Harrison, J. J. Foster and Z. Bruce, Int. J. Mass Spectrom., 2009, 286, 53–63.

29 D. A. Sverjensky and N. Lee, Elements, 2010, 6, 31–36.

30 J. M. Mattinson, Chem. Geol., 2005, 220, 47–66.

31 B. Schoene, J. L. Crowley, D. J. Condon, M. D. Schmitz and S. A. Bowring, Geochim. Cosmochim. Acta, 2006, 70, 426–445.

32 A. Verbruggen, A. Alonso, R. Eykens, F. Kehoe, H. Kuhn, S. Richter and Y. Aregbe, JRC Scientific and Technical Reports, 2008.

33 S. Weyer, A. D. Anbar, A. Gerdes, G. W. Gordon, T. J. Algeo and E. A. Boyle, *Geochim. Cosmochim. Acta*, 2008, **72**, 345–359.

34 E. Horwitz, M. Dietz, R. Chiarizia, H. Diamond, A. Essling and D. Graczyk, *Anal. Chim. Acta*, 1992, **266**, 25–37.

35 K. M. Samperton, B. Schoene, J. M. Cottle, C. B. Keller, J. L. Crowley and M. D. Schmitz, *Chem. Geol.*, 2015, **417**, 322–340.

36 S. Richter, R. Eykens, H. Kuhn, Y. Aregbe, A. Verbruggen and S. Weyer, *Int. J. Mass Spectrom.*, 2010, **295**, 94–97.

37 F. L. H. Tissot, C. Chen, B. M. Go, M. Naziemiec, G. Healy, A. Bekker, P. K. Swart and N. Dauphas, *Geochim. Cosmochim. Acta*, 2018, **242**, 233–265.

38 A. P. Meshik, O. V. Pravdivtseva and C. M. Hohenberg, *Phys. Rev. C*, 2016, **93**, 044614.

39 S. E. Bentridi, B. Gall, F. Gauthier-Lafaye, A. Seghour and D. E. Medjadi, *C. R. Geosci.*, 2011, **343**, 738–748.

40 E. Roth, *J. Radioanal. Chem.*, 1977, **37**, 65–78.

41 A. Goldmann, G. Brennecka, J. Noordmann, S. Weyer and M. Wadhwa, *Geochim. Cosmochim. Acta*, 2015, **148**, 145–158.

42 Z. Adam, *Astrobiology*, 2007, **7**, 852–872.

43 M. Blanchard, E. Balan and E. A. Schauble, *Non-Traditional Stable Isotopes*, 2017, vol. 82, pp. 27–63.

44 Y. Fujii, N. Higuchi, Y. Haruno, M. Nomura and T. Suzuki, *J. Nucl. Sci. Technol.*, 2006, **43**, 400–406.

45 R. B. Ickert, R. Mundil, C. W. Magee and S. R. Mulcahy, *Geochim. Cosmochim. Acta*, 2015, **168**, 88–110.

46 K. M. Samperton, E. A. Bell, M. Barboni, C. B. Keller and B. Schoene, *Geology*, 2017, **45**, 983–986.

47 H. R. Halse, PhD thesis, Imperial College London, 2014.

48 F. Farges, C. W. Ponader, G. Calas and G. E. Brown, *Geochim. Cosmochim. Acta*, 1992, **56**, 4205–4220.

49 D. Trail, E. B. Watson and N. D. Tailby, *Nature*, 2011, **480**, 79–U238.

50 J. M. Hanchar, *Rev. Mineral.*, 1999, **38**, 499–519.

51 F. Farges and G. Calas, *Am. Mineral.*, 1991, **76**, 60–73.

52 E. R. Vance and D. J. Mackey, *J. Phys. C: Solid State Phys.*, 1974, **7**, 1898–1908.

53 M. Tiepolo, R. Oberti and R. Vannucci, *Chem. Geol.*, 2002, **191**, 105–119.

54 A. M. Seydoux-Guillaume, J. L. Paquette, M. Wiedenbeck, J. M. Montel and W. Heinrich, *Chem. Geol.*, 2002, **191**, 165–181.

55 T. M. Harrison, E. B. Watson and A. B. Aikman, *Geology*, 2007, **35**, 635–638.

56 J. A. Whitney and J. C. Stormer, *J. Petrol.*, 1985, **26**, 726–762.

57 B. R. Frost, K. R. Chamberlain and J. C. Schumacher, *Chem. Geol.*, 2001, **172**, 131–148.

58 A. von Quadt, J. F. Wotzlaw, Y. Buret, S. J. E. Large, I. Peytcheva and A. Trinquier, *J. Anal. At. Spectrom.*, 2016, **31**, 658–665.

59 J. F. Wotzlaw, Y. Buret, S. J. E. Large, D. Szymanowski and A. von Quadt, *J. Anal. At. Spectrom.*, 2017, **32**, 579–586.

60 M. D. Schmitz and S. A. Bowring, *Geochim. Cosmochim. Acta*, 2001, **65**, 2571–2587.

61 J. H. F. L. Davies and L. M. Heaman, *Precambrian Res.*, 2014, **249**, 180–198.

62 G. R. Tilton and M. H. Grunenfelder, *Science*, 1968, **159**, 1458–1461.

63 D. P. Hawkins and S. A. Bowring, *Contrib. Mineral. Petrol.*, 1999, **134**, 150–169.

64 M. D. Schmitz and B. Schoene, *Geochem., Geophys., Geosyst.*, 2007, **8**(8), Q08006.

65 N. M. McLean, J. F. Bowring and S. A. Bowring, *Geochem., Geophys., Geosyst.*, 2011, **12**(6), Q0AA18.

66 L. M. Fairchild, N. L. Swanson-Hysell, J. Ramezani, C. J. Sprain and S. A. Bowring, *Lithosphere*, 2017, **9**, 117–133.

67 M. Barboni, P. Boehnke, B. Keller, I. E. Kohl, B. Schoene, E. D. Young and K. D. McKeegan, *Sci. Adv.*, 2017, **3**, e1602365.

68 J. L. Crowley, B. Schoene and S. A. Bowring, *Geology*, 2007, **35**, 1123–1126.

69 A. Trinquier, C. Maden, A. L. Faure, A. Hubert, F. Pointurier, B. Bourdon and M. Schonbachler, *Anal. Chem.*, 2019, **91**, 6190–6199.

70 B. Schoene, M. J. de Wit and S. A. Bowring, *Tectonics*, 2008, **27**(5), TC5010.

71 B. Schoene and S. A. Bowring, *Geol. Soc. Am. Bull.*, 2010, **122**, 408–429.

72 M. Barboni and B. Schoene, *Nat. Geosci.*, 2014, **7**, 524–528.

73 W. C. Clyde, P. Wilf, A. Iglesias, R. L. Slingerland, T. Barnum, P. K. Bijl, T. J. Bralower, H. Brinkhuis, E. E. Comer, B. T. Huber, M. Ibanez-Mejia, B. R. Jicha, J. M. Krause, J. D. Schueth, B. S. Singer, M. S. Raigemborn, M. D. Schmitz, A. Sluijs and M. D. Zamaloa, *Geol. Soc. Am. Bull.*, 2014, **126**, 289–306.

74 N. L. Swanson-Hysell, S. D. Burgess, A. C. Maloof and S. A. Bowring, *Geology*, 2014, **42**, 475–478.

75 M. Barboni, C. Annen and B. Schoene, *Earth Planet. Sci. Lett.*, 2015, **432**, 436–448.

76 S. D. Burgess and S. A. Bowring, *Sci. Adv.*, 2015, **1**, e1500470.

77 S. D. Burgess, S. A. Bowring, T. H. Fleming and D. H. Elliot, *Earth Planet. Sci. Lett.*, 2015, **415**, 90–99.

78 W. C. Clyde, J. Ramezani, K. R. Johnson, S. A. Bowring and M. M. Jones, *Earth Planet. Sci. Lett.*, 2016, **452**, 272–280.

79 C. D. Deering, B. Keller, B. Schoene, O. Bachmann, R. Beane and M. Ovtcharova, *Geology*, 2016, **44**, 267–270.

80 M. P. Eddy, S. A. Bowring, P. J. Umhoefer, R. B. Miller, N. M. McLean and E. E. Donaghy, *Geol. Soc. Am. Bull.*, 2016, **128**, 425–441.

81 M. P. Eddy, S. A. Bowring, R. B. Miller and J. H. Tepper, *Geology*, 2016, **44**, 331–334.

82 J. M. Husson, B. Schoene, S. Bluher and A. C. Maloof, *Earth Planet. Sci. Lett.*, 2016, **436**, 108–120.

83 C. E. Bucholz, M. P. Eddy, O. Jagoutz, S. A. Bowring, M. W. Schmidt and O. Sambuu, *Geology*, 2017, **45**, 11–14.

84 M. P. Eddy, K. P. Clark and M. Polenz, *Lithosphere*, 2017, **9**, 652–664.

85 M. P. Eddy, O. Jagoutz and M. Ibanez-Mejia, *Geology*, 2017, **45**, 527–530.

86 E. B. Harris, C. A. E. Stromberg, N. D. Sheldon, S. Y. Smith and M. Ibanez-Mejia, *Geol. Soc. Am. Bull.*, 2017, **129**, 1241–1251.

This journal is © The Royal Society of Chemistry 2019

J. Anal. At. Spectrom., 2019, **34**, 2035–2052 | 2051

87 J. M. Krause, W. C. Clyde, M. Ibanez-Mejia, M. D. Schmitz, T. Barnum, E. S. Bellosi and P. Wilf, *Geol. Soc. Am. Bull.*, 2017, **129**, 886–903.

88 A. J. Schaen, J. M. Cottle, B. S. Singer, C. B. Keller, N. Garibaldi and B. Schoene, *Geology*, 2017, **45**, 835–838.

89 J. Kasbohm and B. Schoene, *Sci. Adv.*, 2018, **4**(9), eaat8223.

90 S. MacLennan, Y. Park, N. Swanson-Hysell, A. Maloof, B. Schoene, M. Gebreslassie, E. Antilla, T. Tesema, M. Alene and B. Haileab, *Geology*, 2018, **46**, 539–542.

91 B. C. Ratschbacher, C. B. Keller, B. Schoene, S. R. Paterson, J. L. Anderson, D. Okaya, K. Putirka and R. Lippoldt, *J. Petrol.*, 2018, **59**(9), 1787–1809.

92 S.-Z. Shen, J. Ramezani, J. Chen, C.-Q. Cao, D. H. Erwin, H. Zhang, L. Xiang, S. D. Schoepfer, C. M. Henderson, Q.-F. Zheng, S. A. Bowring, Y. Wang, X.-H. Li, X.-D. Wang, D.-X. Yuan, Y.-C. Zhang, L. Mu, J. Wang and Y.-S. Wu, *Geol. Soc. Am. Bull.*, 2018, **131**(1–2), 205–223.

93 M. P. Eddy, M. Ibanez-Mejia, S. D. Burgess, M. A. Coble, U. G. Cordani, J. DesOrmeau, G. E. Gehrels, X. H. Li, S. MacLennan, M. Pecha, K. Sato, B. Schoene, V. A. Valencia, J. D. Vervoort and T. T. Wang, *Geostand. Geoanal. Res.*, 2019, **43**, 113–132.

94 N. L. Swanson-Hysell, J. Ramezani, L. M. Fairchild and I. R. Rose, *Geol. Soc. Am. Bull.*, 2019, **131**(5–6), 913–940.

95 A. H. Jaffey, K. F. Flynn, L. E. Glendenin, W. C. Bentley and A. M. Essling, *Phys. Rev. C*, 1971, **4**, 1889–1906.